Materials Physics and Mechanics. 2023;51(7): 63-98
Research article
http://dx.doi.org/10.18149/MPM.572023_7

Submitted: September 21, 2022
Approved: February 22, 2023
Accepted: July 13, 2023

Modal and harmonic analysis of the rotor system involving four different materials by finite element code: Ansys workbench

N.E.B. Afane [1], S. Zahaf [2]✉, M. Dahmane [3], A. Belaziz [4], R. Noureddine [5]

[1] National Polytechnic School of Oran, Oran, Algeria

[2] University of Djilali Bounaama-Khamis Meliana, Ain Defla, Algeria

[3] Higher National School of Hydraulics, Blida, Algeria

[4]Mechanical Research Center Constantine (CRM), Constantine, Algeria

[5] University of Oran 2 Mohamed Ben Ahmed, Oran, Algeria

✉ samir.zahaf@univ-dbkm.dz

Abstract. This article presents the study of the Jeffcott rotor shaft system, diameter 32 mm, length 1000 mm with a disc in the middle of an exterior diameter 250 and 30 mm thickness for four different materials namely (JIS-S45C steels, 38CrMoAl steels, structural steels, titanium steels (Ti-6AL-4V)), for a case simply supported, and it is important to determine the natural frequencies, critical speeds and amplitudes of the rotor system (von Mises stress, principal stress, maximum shear stress, lifetime). This characteristic is found by using the parametric design tool ANSYS Workbench. Modal, harmonic cases are realized for the single-rotor system. The results obtained for this analysis are useful for design of rotor system and to facilitate engineering applications and allied researches by presenting a detailed comparative picture based on dynamic analysis of Jeffcott rotor. The authors covered modal, harmonic response along with natural frequencies and whirling speeds at different modes. Resonance occurrence speeds are also analyzed using the Campbell diagram. The harmonic response is investigated, with added material (0.1 kg) on the disc, to reveal the von Mises stress, normal elastic strain, total displacement, maximum shear stress and life cycle number. FEA is carried out to estimate critical speeds for these four materials. The results of this study indicated that the critical speeds are superiors for 38CrMoAl steel, (1858.7, 1859.4, 8468.1 rpm) and lower for the steels of JIS-S45C (1784.2, 1784.9, 8147.7 rpm) by contribution the two steels (structural steels, titanium alloy (Ti-6Al-4V)). The natural frequencies of the Jeffcott rotor are also higher for 38CrMoAl steels and are equal for the two materials (Titanium alloy (Ti-6Al-4V), JIS-S45C) and minimum for structural steels. On the other hand, the results of the harmonic analysis indicated that the vibration severity is very lower for 38CrMoAl steels material (9435.2 MPa) and very higher for structural steels material (55134 MPa). The rotary machines undergoing high stress severity and deformation severity are recommended to use 38CrMoAl steels. Rotor dynamic analysis of Jeffcott rotor with four materials, JIS-S45C, 38CrMoAl, structural steel, titanium alloy materials are highly recommended with the less severity of vibration. Choose JIS-S45C and 38CrMoAl materials for higher whirling speeds compared to structural steel, titanium alloy materials. The rotary machines undergoing higher operating speeds like propeller shafts, turbine and compressor are recommended to use JIS S45C and 38CrMoAl.

Keywords: rotor; natural frequency; critical speeds; amplitudes; phase angle; damping; Von Mises stress; strain elastic; total displacement

Citation: Afane NEB, Zahaf S, Dahmane M, Belaziz A, Noureddine R. Modal and harmonic analysis of the rotor system involving four different materials by finite element code: Ansys workbench. *Materials Physics and Mechanics*. 2023;51(7): 63-98. DOI: 10.18149/MPM.5172023_7.

Publisher: Peter the Great St. Petersburg Polytechnic University

Introduction

Rotor Dynamics is a branch of physics which deals with study of behaviour of rotating systems under application of dynamic forces. Rotor is part of system i.e. disks, blades or couplings mounted on shaft is called as rotor. Rotor is used to convert one form of energy into another form hence rotational energy must be maximum, so we must reduce vibrational energy as much as possible, so they have wide range of applications in many industries as well as household applications so we need to analyse the system to prevent catastrophic failures.

Applications such as centrifugal pumps, generators, motors, compressors, blowers, sewing machine, steam turbines, gas turbines, aero engines, main and tail rotors of helicopters. In rotating system, flexural vibrations are main cause as compared to torsional vibration and axial vibration.

Unbalance in rotor gives raise to forces and moments in rotor, this generates flexural vibration in rotor. The vibrations perpendicular to the axis of rotation, such vibrations are known as flexural vibrations. Whirling is one of the main cause for failures of rotating systems due unbalance of rotor i.e. due to the manufacturing defects center of gravity of shaft doesn't coincide with axis of rotation, misalignment of rotor shaft and bearings, due to loose supports or if the machine is operated at critical speeds may lead to catastrophic failure of system.

Generally, rotors rotate at high speeds, when the natural frequency of the system is equal to the critical speed resonance occur. Resonance is the most common problem in rotating systems. In a rotating system, if there is some percentage of vibration in the machine, these vibrations are magnified by resonance. At these critical speeds the amplitude of vibration goes on increasing this cause rotor to bend and twist so this cause rubs or wear and tear and collide with adjacent parts of system hence excessive force are developed and hence leads to failure. So determination of natural frequency, critical speeds and amplitudes of vibrations are very important in rotor dynamics. As a designer by changing mass, stiffness, position of disk etc. such design modification to change critical speeds of system to operate in a suitable environment. To reduce whirling amplitudes, we must avoid rotating at critical speeds of the system, or squeeze film damper is suitable. By using damper, whirling amplitudes are reduced as well as reduces forces on the supports [1].

Tai et al. [2] analysed steady state response of a single rub-impact rotor system. The harmonic balance method with pseudo arc-length continuation is used to obtain the analytical solutions of the stable periodic motion. The changed of frequency response due to unbalance at first natural frequency was discussed. Nanfei Wang and Dongxiang Jiang [3] described vibration response characteristics of a dual rotor unbalance. The governing equation of dual rotor system with unbalance was numerically derived by using Runge Kutta method. The rotor test rig model was conducted to experimentally validate the responses due to the rotating unbalance. Juan Xu et al. [4] presented vibration characteristics of unbalance responses for motorized spindle system using mathematical and simulation models at high excitation frequencies. SM Ghoneam et al. [5] studied the dynamic analysis of a rotor system with active magnetic bearings. This system consists of a flexible shaft with a rigid disk and flexible bearings. Natural frequencies of rotor active magnetic bearings system are evaluated using Ansys Workbench and finite element based on Matlab code. Natural frequencies and mode shapes are evaluated in the case of free-free system and with AMB stiffness at rotational speed $\Omega=0$. The results show that the natural frequencies increase with the increase of bearing stiffness. The higher modes do not differ much when the bearing stiffness increases. Stiffness of AMB increases with the increase in both current and number of turns, and decreases with the increase in the air gap. Comparison between results that obtained from Ansys Workbench and finite element and the error percentages between them has been illustrated. Very close agreement has been obtained. The results which obtained from Ansys Workbench are more accurate.

Amit Malgol et al. [1] studied and analysed of rotor shaft system for three different position of the disk, for a simply supported case, and it is important to determine natural frequency, critical speeds and amplitudes of rotor system. This characteristic is found by using ANSYS parametric design tool. Modal, harmonic and transient cases are carried out for the single rotor system. The results obtained for this analysis are useful for design of rotor system. The results obtained from analytical method have close agreement with the results obtained from ANSYS results.

Emna Sghaier et al. [6] created a new mathematical model for the dynamic behavior of the rotating machines at non-stationary regime shows coupling between the lateral and torsional degrees of freedom. It also shows strong non-linearities. The results of the simulations show that the model help to better understand the behavior of the rotating machinery. It shows the interaction between the rotational behavior and the lateral one, especially in the vicinity of the critical speed.

Yuanchang Chen et al. [7] studied a comprehensive experimental and numerical study based on three modal tests and a correlated finite element simulation to study the complex curvature mode shapes and mode coupling dynamics for a three bladed wind turbine assembly. Three tests are conducted: Test 1, ten accelerometers are deployed on the whole assembly under impact excitation; Test 2, nine accelerometers are deployed on a single blade under impact excitation; and Test 3, a non-contact 3D Scanning Laser Doppler Vibrometer (SLDV) test is performed on a single blade under shaker excitation. The results show that this model has an excellent correlation with both experimental mode shapes from the SLDV test and dynamic response from the impact test. All blade modes below 100 Hz are studied, and experimental and numerical modes give close frequency and well correlated mode shapes.

Mohamed Amine Dabachi et al. [8] studied the durability of Darrieus-type floating wind turbine blades with three-stage rotors under extreme load conditions. Considering the applied stresses, perfect long-term durability is required. FEM allows the selection of materials (fiber, matrix), fiber architectures (plies, tissues), and the optimization of lay-up sequences that minimize the sensitivity to mechanical stresses applied to the structures. The results show that the composite materials, with proper ply orientation, are the best choice to achieve these characteristics. These characteristics result in a high strength-to-weight ratio, which reduces the total weight of the blade and the centrifugal forces acting on it.

Arnab Bose et al. [9] analyzed the natural and whirl frequencies of a slant-cracked functionally graded rotor-bearing system using finite element analysis for the flexural vibrations. The functionally graded shaft is modelled using two nodded beam elements formulated using the Timoshenko beam theory. The flexibility matrix of a slant-cracked functionally graded shaft element has been derived using fracture mechanics concepts, which is further used to develop the stiffness matrix of a cracked element. Material properties are temperature and position dependent and graded in a radial direction following power-law gradation. A Python code has been developed to carry out the complete finite element analysis to determine the Eigenvalues and Eigenvectors of a slant-cracked rotor subjected to different thermal gradients. The analysis investigates and further reveals significant effect of the power-law index and thermal gradients on the local flexibility coefficients of slant-cracked element and whirl natural frequencies of the cracked functionally graded rotor system.

For mathematical modelling, D'Alembert's Principle was used to derive the equation of motion and ANSYS was used to simulate the response. Apart from those studies on analysis of vibration response due to rotating unbalance, Sudhakar and Sekhar et al. [10] identified unbalance fault in a rotor bearing system using equivalent loads minimization and vibration minimization method. Unbalance fault was experimentally identified for one rotating speed and three unbalance conditions. The maximum discrepancy was 23% in unbalance identification process. Using different method, Akash Shrivastava and Amiya Ranjan Mohanty et al. [11] also

identified unbalance in a rotor system. Three different rotating speeds and four unbalance conditions were presented using a joint input estimation. The maximum discrepancy between actual and estimated unbalance reported is 10 %. In the present study, Jeffcott rotor is simulated using FEM by ANSYS, and the Whirl map diagrams are plotted. The analytical results are reported with backward whirl when the rotor is coasting down.

Pavlenko et al. [12] aimed to investigating rotor dynamics of multistage centrifugal machines with ball bearings by using the computer programs "Critical frequencies of the rotor" and "Forced oscillations of the rotor," which are implemented the mathematical model based on the use of beam finite elements. Free and forces oscillations of the rotor for the multistage centrifugal oil pump NPS 200-700 are observed by taking into account the analytical dependence of bearing stiffness on rotor speed, which is previously defined on the basis of results' approximation for the numerical simulation in ANSYS by applying 3D finite elements. The calculations found that characteristic and constrained oscillations of rotor and corresponded to them forms of vibrations, as well as the form of constrained oscillation on the actual frequency for acceptable residual unbalance are determined.

Ralston Fernandes et al. [13] presented a methodology for conducting a 3-D static fracture analysis with applications to a gas turbine compressor blade. An open crack model is considered in the study, and crack-tip driving parameters are estimated by using 3-D singular crack-tip elements in ANSYS. The static fracture analysis is verified with a special purpose fracture code (FRANC3D). Results demonstrate that for the applied loading condition, a mixed mode crack propagation is expected. In the modal analysis study, increasing the depth of the crack leads to a decrease in the natural frequencies of both the single blade and bladed disk system, while increasing the rotational velocity increases the natural frequencies. The presence of a crack also leads to mode localization for all mode families, a phenomenon that cannot be captured by a single blade analysis.

Hyung-Chul Jung et al. [14] presented a rotor dynamic modelling and analysis of a radial inflow turbine rotor-bearing system. One of the challenging aspects of radial turbine design and manufacturing is vibration and stability. In this rotor dynamic analysis of a 1 kWe radial inflow turbine, a computer model is constructed for a rotating shaft with a row of rotor blades supported by two ball bearings. The modal and harmonic analyses are performed with the model to determine the design for safe operation of the turbine. The design parameters of the shaft length and diameter, and the distance between two bearings were varied to identify the critical speeds and unbalance response. A parametric study is then conducted on variations in unbalanced force and bearing stiffness.

Work objective and overall methodology

The scientific research objective for this study and the overall methodology as shown in Fig. 1. This article presents the study of the Jeffcott rotor shaft system for four different materials (JIS-S45C steels, 38CrMoAl steels, standard steels, titanium alloy steels (Ti-6AL-4V)), for a case simply supported, and it is important to determine the natural frequencies, critical speeds and amplitudes of the rotor system (von Mises stress, principal stress, maximum shear stress, lifetime). This characteristic is found by using the parametric design tool ANSYS Workbench. Modal, harmonic cases are realized for the single-rotor system. The results obtained for this analysis are useful for the design of the rotor system. In the present work, the dynamic analysis of the rotor is presented with a Jeffcott rotor with a single unbalance mass equal to 0.1 kg. The unbalance mass is symmetrical is mounted on a flexible rotor (see Fig. 2) and on a rigid bearing support and the work is analyzed with the ANSYS Workbench software.

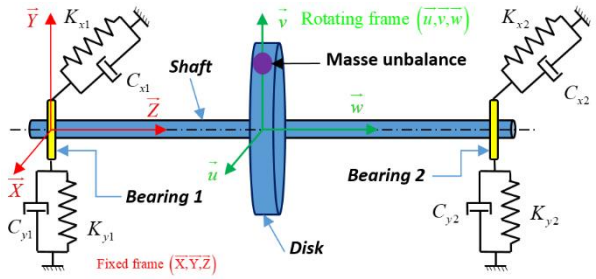

Fig. 1. Dynamic rotor system studied [15]

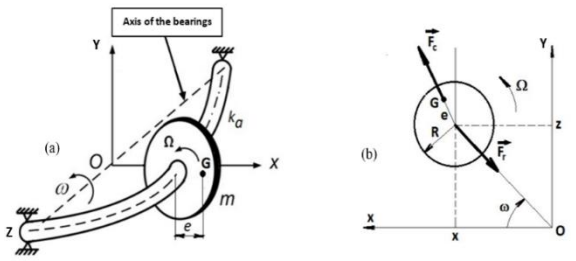

Fig. 2. LAVAL/JEFFCOTT model (a) and plan of oscillations (xoz) (b)

$\overrightarrow{F_c}$ - centrifugal inertial force due to unbalance, $\overrightarrow{F_r}$ - restoring force due to shaft flexibility, e - unbalance eccentricity, R - shaft radius.

In this context, the dynamic characteristics have been analyzed and evaluated where the critical speeds are reported on the basis of the modal analysis, the unbalanced response of the harmonic response, neglecting the gyroscopic effect.

Fundamental equation

The general form of equation of motion for all vibration problems is given by,

$$[M]\{\ddot{u}\} + [C]\{\dot{u}\} + [K]\{u\} = \{f\}, \quad (1)$$

where, symmetric mass matrix $[M] = \begin{pmatrix} m & 0 \\ 0 & m \end{pmatrix}$, symmetric damping matrix $[C] = \begin{pmatrix} c & 2m\omega \\ -2m\omega & c \end{pmatrix}$, symmetric stiffness matrix $[K] = \begin{pmatrix} K & 0 \\ 0 & K \end{pmatrix}$, external force vector $\{f\} = \begin{bmatrix} -mg\sin\theta \\ -mg\cos\theta \end{bmatrix}$ = f(t), generalized coordinate vector in rotordynamics $\{u\}$.

This equation of motion can be expressed in the following general form [3].

$$[M]\{\ddot{u}\} + ([C] + [G])\{\dot{u}\} + ([K] + [B])\{u\} = \{f\}. \quad (2)$$

The above-mentioned equation (2) describes the motion of an axially symmetric rotor, which is rotating at constant spin speed Ω about its spin axis. This equation is just similar to the general dynamic equation except it is accompanied by skew-symmetric gyroscopic matrix, $[G]$ and skew-symmetric circulatory matrix $[B]$. The gyroscopic and circulatory matrices $[G]$ and $[B]$ are greatly influenced by rotational velocity Ω. When the rotational velocity Ω, tends to zero, the skew-symmetric terms present in equation (2) vanish and represent an ordinary stand still structure. The gyroscopic matrix $[G]$ contains inertial terms and that are derived from kinetic energy due to gyroscopic moments acting on the rotating parts of the machine. If this equation is described in rotating reference frame, this gyroscopic matrix $[G]$ also contains the terms associated with Carioles acceleration.

The circulatory matrix $[B]$ is contributed mainly from internal damping of rotating elements [16]. The concept of rotor dynamics can be easily demonstrated with the help of generalized Laval-Jeffcott rotor modal, as shown in Fig. 2.

The generalized Laval-Jeffcott rotor consists of a long, flexible mass less shaft with flexible bearings on both the ends. The bearings have support stiffness of K_x and K_y associated with damping C_x and C_y in x and y direction respectively. There is a massive disk of mass, m located at the center of the shaft. The center of gravity of the disk is offset from the shaft geometric center by an eccentricity of e. The motion of the disk center is described by two translational displacements, (x, y) as shown in Fig. 2 and 3. We consider that:

1. Lateral vibrations are damped;
2. The model is symmetrical;
3. Gravity and the gyroscopic effect are neglected;
4. The rotational speed Ω is constant;
5. The oscillations take place in the plane perpendicular to the plane of equilibrium of the system.

Let's go back to the JEFFCOTT model and consider the flexible and isotropic bearings, i.e. the characteristics are identical in the 2 directions Ox and Oy as shown in Fig. 3.

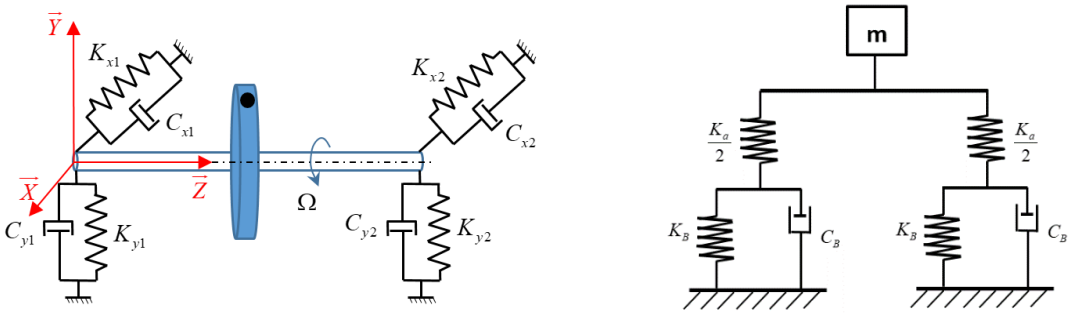

(a) (b)

$$K = K_{x1} = K_{x2} = K_{y1} = K_{y2} = K_x = K_y = K_B = \frac{(2K_a.K_B)}{(2K_a+K_B)} \text{ and } C_x = C_y = 2C_B$$

Fig. 3. Model with flexible and isotropic bearings (a), and oscillator in each direction (b)

When the rotor is rotating at constant rotational speed, the equation of motion for the mass center can be derived from Newton's law of motion, and it is expressed in the following form.

$$m\frac{d^2}{dt^2}(x + e\,cos(\Omega t + \phi_e)) = -C_x\dot{x} - K_x x \quad (3)$$

$$m\frac{d^2}{dt^2}(y + e\,sin(\Omega t + \phi_e)) = -C_y\dot{y} - K_y y \quad (4)$$

The above equations can be re-written as,

$$m\ddot{x} + C_x\dot{x} + K_x x = me\Omega^{2\,cos(\Omega t+\phi_e)}, \quad (5)$$

$$m\ddot{y} + C_y\dot{y} + K_y y = me\Omega^2\,sin(\Omega t + \phi_e), \quad (6)$$

where, is the phase angle of the mass unbalance. The above equations of motions show that the motions in X and Y direction are both dynamically and statically decoupled in this model. Therefore, they can be solved separately.

Determination of natural frequencies. For this simple rotor model, the undamped natural frequency, damping ration and the damped natural frequency of the rotor model for X and Y direction can be calculated from.

$$\omega_{nx} = \sqrt{\frac{K_x}{m}},\ \zeta_x = \frac{C_x}{2m\omega_{nx'}},\ \omega_x = \omega_{nx}\sqrt{1-\zeta_x^2},\ \omega_{ny} = \sqrt{\frac{K_y}{m}},\ \zeta_y = \frac{C_y}{2m\omega_{ny'}},\ \omega_y = \omega_{ny}\sqrt{1-\zeta_y^2} \quad (7)$$

Steady state response to unbalance. For a single unbalance force, as present in this case, that can be set to zero. Therefore, the equations (5) and (6) becomes,

$$m\ddot{x} + C_x\dot{x} + K_x x = me\Omega^2 cos(\Omega t), \quad (8)$$

$$m\ddot{y} + C_y\dot{y} + K_y y = me\Omega^2 sin(\Omega t). \quad (9)$$

Then the solution for the response is,

$$|x| = \frac{me\Omega^2}{\sqrt{[(K_x-\Omega^2 m)^2+(\Omega C_x)^2]}}, \quad (10)$$

$$|y| = \frac{me\Omega^2}{\sqrt{\left[(K_y-\Omega^2 m)^2+(\Omega C_y)^2\right]}}. \quad (11)$$

Rotor-Dynamic Analysis: modal and harmonic

Modal analysis. The role of Modal analysis is to facilitate the investigations pertaining to the vibration characteristics (natural frequencies and mode shapes) of a mechanical structure or component, showing the movement of different parts of the structure under dynamic loading conditions. Modal Analysis offers different modes with natural frequencies and, one can obtain the critical speeds from the whirl map diagram, which are useful to review the stability and resonance occurrence possibility. Its use can be observed in different fields such as rotor dynamic analysis for a hydraulic turbine [17] to chaotic vibration reduction in a centrifugal pump [18]. Modal fitting of different vibration modes and use of frequency response functions facilitate virtual manufacturing setup for the use of structural dynamics concepts [19]. In context to modal analysis, Jeffcott rotor equations of motion are as under, covering forces [20,21].

Harmonic response analysis. The role of harmonic response analysis is to determine responses towards balanced and unbalanced excitations. Many researchers have explored and admired the effectiveness of harmonic response analysis to find results based on various vibration parameters [22-24]. To perform a harmonic analysis of an unbalanced excitation; the effect of the unbalanced mass is represented by the forces in the two perpendicular directions to the spinning axis. For a single mass unbalance, the angle a will be zero and one will get the following expressions for the forces in the XY plane, as shown in Fig. 4:

$$F_x = F_c \cos \Omega t = F_c e^{j\Omega t}, \tag{12}$$

$$F_y = F_c \sin \Omega t = F_c \cos\left(\Omega t - \frac{\pi}{2}\right), \tag{13}$$

where, The Z-axis is a spinning axis, m = unbalance mass, Ω = rotational velocity, r = radius of the eccentric mass, ω = angular velocity of in rad/sec.

Mathemanical modeling

To perform the simulations, is necessary to obtain the mathematical model of the rotor-bearing system, where was used Finite Element Method. Initially it was found the kinetic energy, potential and forces that were applied to the elements of the system, as described by [25].

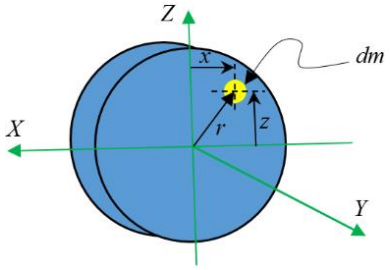

Fig. 4. Representation of disk [27]

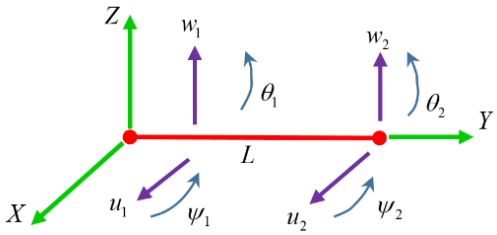

Fig. 5. Modeling of one dimensional (1D) rotor [29]

Finite elements method. According to Rao [26], these methods allow more accurate predictions, reducing the cost of experiments and simulation, thus achieving cheaper and more accurate designs before testing prototypes. Through this method can be found matrices of mass, stiffness, damping, the gyroscopic effect mass and unbalanced. In this method is used the energy equations for each element, and without the generalized coordinates, but with the degrees of freedom available in the element. For the derivation of the equations of motion of the rotor, just apply the Lagrange equation in the kinetic energy, potential and forces of the system, as described by [27]. The general equation is given as:

$$\frac{d}{dt}\left(\frac{\partial T}{\partial \delta}\right) - \frac{\partial T}{\partial \delta} + \frac{\partial U}{\partial \delta} = F, \tag{14}$$

where ($N(1 \le i \le N)$) is the number of degree of freedom, δ is the displacement vector and º indicates differentiation in relation to time. These equation follows a procedure used by [28]. In the case of the disc element, as it has four degrees of freedom, u, w, θ *and* ψ , Fig. 4.

Assuming that the kinetic energy of the disc is obtained using Lagrange has to the following equation:

$$\frac{d}{dt}\left(\frac{\partial T_D}{\partial \delta'}\right) - \frac{\partial T_D}{\partial \delta} = [M_D]\{\delta''\} + \Omega[C_D]\{\delta'\}, \quad (15)$$

where $[M_D]$ is the classical mass matrix and $[C_D]$ is the gyroscopic matrix.

In 1D finite element, the shaft is modeled as a beam which has a constant circular cross-section. If the element has two nodal, it will form the 8- order matrix. Each of the nodal has 4 degrees of freedom: 2 displacements and 2 slopes in both x-y plane and y-z planes (Fig. 5), therefore nodal displacement vector can be written in the equation [29]. To shaft matrices, first is shown that this have to be divided through nodes, as shown in Fig. 5:

$$\delta = [u_1, w_1, \theta_1, \Psi_1, u_2, w_2, \theta_2, \Psi_2]^T. \quad (16)$$

The relationship between displacement and slope are:

$$\theta = \frac{\delta w}{\delta y}, \quad (17)$$

$$\Psi = -\frac{\delta u}{\delta y}. \quad (18)$$

Displacements δu and δw in accordance with movements in the X and Y directions written by the equation:

$$\delta u = [u_1, \Psi_1, u_2, \Psi_2]^T, \quad (19)$$

$$\delta w = [w_1, \theta_1, w_2, \theta_2]^T. \quad (20)$$

Displacements in the finite element are formed from:

$$u = N_1(y)\delta u, \quad (21)$$

$$w = N_2(y)\delta w. \quad (22)$$

$N_1(y)$ and $N_2(y)$ are the function of displacements for the beam that are subjected to bending loads:

$$N_1(y) = \left[1 - \frac{3y^2}{L^2} + \frac{2y^3}{L^3}; -y + \frac{2y^2}{L} - \frac{y^3}{L^2}; \frac{3y^2}{L^2} - \frac{2y^3}{L^3}; \frac{y^2}{L} - \frac{y^3}{L^2}\right], \quad (23)$$

$$N_2(y) = \left[1 - \frac{3y^2}{L^2} + \frac{2y^3}{L^3}; y - \frac{2y^2}{L} + \frac{y^3}{L^2}; \frac{3y^2}{L^2} - \frac{2y^3}{L^3}; -\frac{y^2}{L} + \frac{y^3}{L^2}\right]. \quad (24)$$

Kinetic energy of the shaft can be calculated as [29]:

$$T = \frac{\rho S}{2}\int_0^L [\delta\dot{u}^T N_1^T N_1 \delta\dot{u} + \delta\dot{w}^T N_2^T N_2 \delta\dot{w}]\, dy + \frac{\rho I}{2}\int_0^L \left[\delta\dot{u}^T \frac{dN_1^T}{dy}\frac{dN_1}{dy}\delta\dot{u} + \right.$$

$$\left. + \delta\dot{w}^T \frac{dN_2^T}{dy}\frac{dN_2}{dy}\delta\dot{w}\right] dy - 2\rho I\Omega \int_0^L \delta\dot{u}^T \frac{dN_1^T}{dy}\frac{dN_2}{dy}\delta w dy + \rho IL\Omega^2, \quad (25)$$

where ρ is the density, S is the cross-sectional area of the beam, and N shape functions, I is the area moment of inertia of the beam cross-section about the neutral axis, Ω angular velocity and L is the length of the element. Making the necessary integrations and applying Lagrange, is obtained. Substitution of equation (23) and (24) into equation (25), then [27]:

$$T = \frac{1}{2}\delta\dot{u}^T M_1 \delta\dot{u} + \frac{1}{2}\delta\dot{w}^T M_2 \delta\dot{w} + \frac{1}{2}\delta\dot{u}^T M_3 \delta\dot{u} + \frac{1}{2}\delta\dot{w}^T M_4 \delta\dot{w} + \Omega\delta\dot{u}^T M_5 \delta w + \rho IL\Omega^2, \quad (26)$$

where M_1 and M_2 are the classical mass matrix, M_3 and M_4 are generated due to a secondary effect of rotor inertia, and M_5 is generated due to gyroscopic. By applying the Lagrange equation, then [27]:

$$\frac{d}{dt}\left(\frac{\partial T}{\partial \dot{\delta}}\right) - \frac{\partial T}{\partial \delta} = (M + M_s)\ddot{\delta} + C\dot{\delta}, \quad (27)$$

where $[M]$ is the classical mass matrix, $[M_S]$ effect of inertia matrix and $[C_S]$ gyroscopic matrix. Where M and M_s are obtained from M_1, M_2, M_3, M_4 and C from M_5, thus [27]:

$$M=\frac{\rho SL}{420}\begin{bmatrix}156 & 0 & 0 & -22L & 54 & 0 & 0 & 13L\\ 0 & 156 & 22L & 0 & 0 & 54 & -13L & 0\\ 0 & 22L & 4L^2 & 0 & 0 & 13L & -3L^2 & 0\\ -22L & 0 & 0 & 4L^2 & -13L & 0 & 0 & -3L^2\\ 54 & 0 & 0 & -13L & 156 & 0 & 0 & 22L\\ 0 & 54 & 13L & 0 & 0 & 156 & -22L & 0\\ 0 & -13L & -3L^2 & 0 & 0 & -22L & 4L^2 & 0\\ 13L & 0 & 0 & -3L^2 & 22L & 0 & 0 & 4L^2\end{bmatrix}, \tag{29}$$

$$M_S=\frac{\rho I}{30L}\begin{bmatrix}36 & 0 & 0 & -3L & -36 & 0 & 0 & -3L\\ 0 & 36 & 3L & 0 & 0 & -36 & 3L & 0\\ 0 & 3L & 4L^2 & 0 & 0 & -3L & -L^2 & 0\\ -3L & 0 & 0 & 4L^2 & 3L & 0 & 0 & -L^2\\ -36 & 0 & 0 & 3L & 36 & 0 & 0 & 3L\\ 0 & -36 & -3L & 0 & 0 & 36 & -3L & 0\\ 0 & 3L & -L^2 & 0 & 0 & -3L & 4L^2 & 0\\ -3L & 0 & 0 & -L^2 & 3L & 0 & 0 & 4L^2\end{bmatrix}, \tag{30}$$

$$C=\frac{\rho I\Omega}{15L}\begin{bmatrix}36 & 0 & 0 & -3L & -36 & 0 & 0 & -3L\\ 0 & 36 & 3L & 0 & 0 & -36 & 3L & 0\\ 0 & 3L & 4L^2 & 0 & 0 & -3L & -L^2 & 0\\ -3L & 0 & 0 & 4L^2 & 3L & 0 & 0 & -L^2\\ -36 & 0 & 0 & 3L & 36 & 0 & 0 & 3L\\ 0 & -36 & -3L & 0 & 0 & 36 & -3L & 0\\ 0 & 3L & -L^2 & 0 & 0 & -3L & 4L^2 & 0\\ -3L & 0 & 0 & -L^2 & 3L & 0 & 0 & 4L^2\end{bmatrix}. \tag{31}$$

Strain energy on the shaft can be calculated by the equation **[27]**:

$$U=\frac{EI}{2}\int_0^L\left[\delta u^T\frac{d^2N_1^T}{dy^2}\frac{d^2N_1}{dy^2}\delta u+\delta w^T\frac{d^2N_2^T}{dy^2}\frac{d^2N_2}{dy^2}\delta w\right]dy + \frac{F_0}{2}\int_0^L\left[\delta u^T\frac{dN_1^T}{dy}\frac{dN_1}{dy}\delta u+\delta w^T\frac{dN_2^T}{dy}\frac{dN_2}{dy}\delta w\right]dy. \tag{32}$$

Then, after integration :

$$U=\frac{1}{2}\delta u^TK_1\delta u+\frac{1}{2}\delta w^TK_2\delta w+\frac{1}{2}\delta u^TK_3\delta u+\frac{1}{2}\delta w^TK_4\delta w, \tag{33}$$

where $[K_1]$and $[K_2]$are the classical stiffness matrix $[K_c]$, $[K_3]$and $[K_4]$are the matrix due to the axial force (K_f). The effect of shear force can be calculated by the equation [27]:

$$a=\frac{12EI}{GS_rL^2}. \tag{34}$$

With shear modulus [27]:

$$G=\frac{E}{2(1+\upsilon)}, \tag{35}$$

where υ is the Poissons ratio and E is Young's modulus of the material. Then by applying Eq. (32) to the Lagrange equation [27]:

$$\frac{\partial U}{\partial\delta}=K\delta, \tag{36}$$

$$K=K_C+K_F, \tag{37}$$

where $[K_c]$and $[K_F]$, can be calculated [27]:

$$K_C = \frac{EI}{(1+a)L^3}\begin{bmatrix} 12 & 0 & 0 & -6L & -12 & 0 & 0 & -6L \\ 0 & 12 & 6L & 0 & 0 & -12 & 6L & 0 \\ 0 & 6L & (4+a)L^2 & 0 & 0 & -6L & (2-a)L^2 & 0 \\ -6L & 0 & 0 & (4+a)L^2 & 6L & 0 & 0 & (2-a)L^2 \\ -12 & 0 & 0 & 6L & 12 & 0 & 0 & 6L \\ 0 & -12 & -6L & 0 & 0 & 12 & -6L & 0 \\ 0 & 6L & (2-a)L^2 & 0 & 0 & -6L & (4+a)L^2 & 0 \\ -6L & 0 & 0 & (2-a)L^2 & 6L & 0 & 0 & (4+a)L^2 \end{bmatrix}, \quad (38)$$

$$K_F = \frac{F}{30L}\begin{bmatrix} 36 & 0 & 0 & -3L & -36 & 0 & 0 & -3L \\ 0 & 36 & 3L & 0 & 0 & -36 & 3L & 0 \\ 0 & 3L & 4L^2 & 0 & 0 & -3L & -L^2 & 0 \\ -3L & 0 & 0 & 4L^2 & 3L & 0 & 0 & -L^2 \\ -36 & 0 & 0 & 3L & 36 & 0 & 0 & 3L \\ 0 & -36 & -3L & 0 & 0 & 36 & -3L & 0 \\ 0 & 3L & -L^2 & 0 & 0 & -3L & 4L^2 & 0 \\ -3L & 0 & 0 & -L^2 & 3L & 0 & 0 & 4L^2 \end{bmatrix}. \quad (39)$$

Moreover, the disc is the main element of the rotor system, which is characterized only by its kinetic energy. The node of the rotor has four degrees of freedom : two displacements u and w and two slopes about the x-y and y-z planes, which are θ and ψ respectively. Then if the nodal displacement vector δ of the center of the disk is [30]:

$$\delta = [u, w, \theta, \Psi]^T. \quad (40)$$

By applying the Lagrange equations, the equation for the disk:

$$\frac{d}{dt}\left(\frac{\partial T}{\partial \dot{\delta}}\right) - \frac{\partial T}{\partial \delta} = \begin{bmatrix} M_D & 0 & 0 & 0 \\ 0 & M_D & 0 & 0 \\ 0 & 0 & I_{Dx} & 0 \\ 0 & 0 & 0 & I_{Dx} \end{bmatrix}\begin{bmatrix} \ddot{u} \\ \ddot{w} \\ \ddot{\theta} \\ \ddot{\Psi} \end{bmatrix} + \Omega\begin{bmatrix} 0 & 0 & 0 & 0 \\ 0 & 0 & 0 & 0 \\ 0 & 0 & 0 & -I_{Dy} \\ 0 & 0 & I_{Dy} & 0 \end{bmatrix}\begin{bmatrix} \dot{u} \\ \dot{w} \\ \dot{\theta} \\ \dot{\Psi} \end{bmatrix}. \quad (41)$$

where the first matrix is the classical stiffness matrix and the second one is the matrix due to gyroscopic effects. In this study, the effects of bearing influence are neglected so that the general equation of rotor dynamics is [30]:

$$M\ddot{\delta} + K\delta = F(t), \quad (42)$$

where δ is all nodal displacement vectors, M is the mass matrix, K is the stiffness matrix and $F(t)$ is the force vector. 1D finite element analysis in this study uses the discretization of 3 elements and 4 nodal. Simplification scheme of the rotor with dimension in mm is shown in Fig. 6.

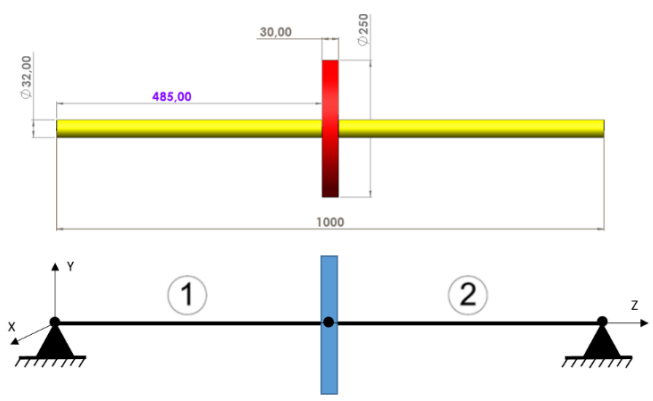

Fig. 6. Simplification scheme of the discretization in 1D finite element analysis for the rotor

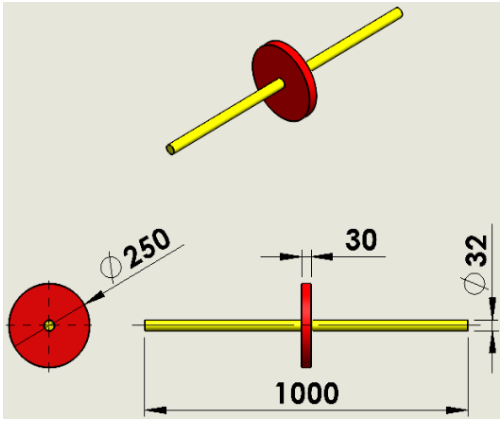

Fig. 7. Jeffcott rotor model definition drawing (using Solidworks)

To produce the equality throughout the element, the local element matrix of each element is arranged into a global matrix. Every element, which has the same number of nodal and that of degrees of freedom, is placed on the same row and column and this applies to the mass matrix, stiffness matrix and damping matrix [27]. The illustrative example of the element assembly from local elements into global element for two local elements can be seen in Fig. 6. Globalizing matrix in this way is the fastest and easy, even for a lot of elements and nodal degrees of freedom. In addition to the dimensions of each component of the rotor, the mechanical properties of the component are also required as the input data of the calculation.

As for bearing is simpler to find the matrix, because having the force equation, the matrix is obtained directly:

$$\begin{bmatrix} F_u \\ F_\theta \\ F_\omega \\ F_\Psi \end{bmatrix} = -\begin{bmatrix} k_{xx} & 0 & k_{xz} & 0 \\ 0 & 0 & 0 & 0 \\ k_{zx} & 0 & k_{zz} & 0 \\ 0 & 0 & 0 & 0 \end{bmatrix} \begin{bmatrix} u \\ \theta \\ \omega \\ \psi \end{bmatrix} - \begin{bmatrix} c_{xx} & 0 & c_{xz} & 0 \\ 0 & 0 & 0 & 0 \\ c_{zx} & 0 & c_{zz} & 0 \\ 0 & 0 & 0 & 0 \end{bmatrix} \begin{bmatrix} \dot{u} \\ \dot{\theta} \\ \dot{\omega} \\ \dot{\psi} \end{bmatrix}. \quad (43)$$

Considering the first the matrix of stiffness and the second matrix of damping, where they can be symmetric, when $k_{xx} = k_{yy}$ et $c_{xx} = c_{yy}$ or asymmetric when $k_{xx} \neq k_{yy}$ et $c_{xx} \neq c_{yy}$.

In the case of unbalanced mass matrix is also obtained directly, applying the Lagrange in the equation kinetic energy of the unbalanced mass, we obtain the following matrix.

$$\begin{bmatrix} F_u \\ F_\omega \end{bmatrix} = m_u d\Omega^2 \begin{bmatrix} cos(\Omega t + \alpha) \\ sin(\Omega t + \alpha) \end{bmatrix}, \quad (43)$$

where Ω is the angular velocity and α is the angular position with respect z axis.

Analysis by 3D finite element method of the rotor dynamics system

Jeffcott rotor geometry and mechanical properties of materials. The program Solidworks, seen in Fig. 7, is used to create the Jeffcott rotor model. The shaft's dimensions are L = 1000 mm in length and d = 32 mm in diameter. Bearings on both ends of the shaft support the rotor. The center is mounted with a disc that has an offset mass of 0.1 kg. The disc has the following measurements: 250 mm in diameter, 30 mm in thickness, and an equal mass unbalance (0.1 kg). A geometric shaft center and an eccentricity of e separate the unbalance's center of gravity from each other. The CAD model and schematic design of the Jeffcott rotor are shown in Figs. 8 and 9. Table 1 depicts the material characteristics. Engineering materials utilized primarily in rotor machines, such as low-carbon steels (JIS-S45C steel, 38CrMoAl steel, structural steel, and titanium alloy steel (Ti-6AL-4V)), were included by the authors.

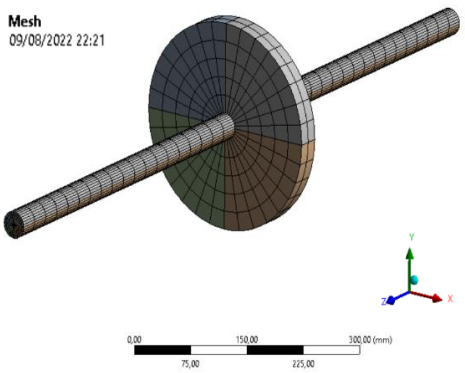

Fig. 8. Global mesh of the Jeffcott rotor model

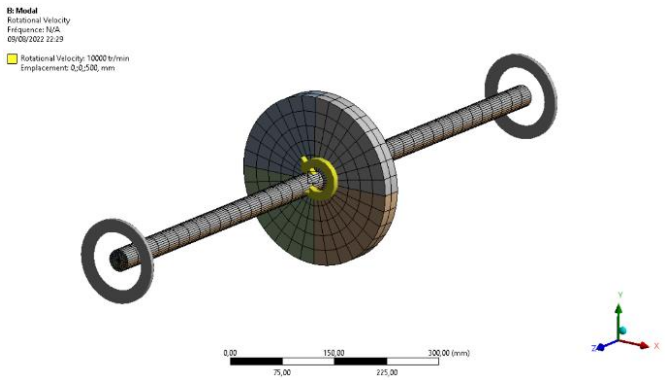

Fig. 9. Boundary conditions of the Jeffcott rotor model: modale analysis

Table 1. Material properties of 4 steels.

Sl.no:	Properties	JIS-S45C steel	38CrMoAl steel	Structure steel	Ti-6Al-4V alloy steel	Units
1	Density	7700	7850	7850		Kg/m^3
2	Young's modulus	190	210	200	114	GPa
3	Poisson's ratio	0,27	0.3	0.3	0.35	Unit less quantity
4	Shear modulus	7.4803E+10	8.0769E+10	7.6923E+10	4.2222E+10	Pa
5	Tensile strength, ultimate	569	571	460	1170	MPa
6	Tensile strength	343	439	250	1100	MPa
7	Elongation at break	20	10	23	10	%
8	Bearing stiffness	1.6e+006	1.6e+006	1.6e+006	1.6e+006	N/mm
9	Bearing damp	23000	23000	23000	23000	N·s/mm
10	Mass	17.346	17.346	17.346	17.346	kg

Jeffcott rotor mesh by Ansys Workbench. Given that the geometry of the product is broken down into a limited number of pieces, meshing is an essential component of ANSYS and works with computer-aided design and engineering processes. The fundamental principle of FEA is to do calculations at a finite set of points and then extrapolate the outcomes to the full volume. Every continuous object has a potentially huge number of degrees of freedom, which could make it difficult to discover solutions by FEA through the use of discretization or meshing, FEA reduces degrees of freedom from infinite to finite. The geometry for the selected Jeffcott rotor with shaft includes 8537 elements with a dimension of 7 mm and 28,682 nodes (details of which have already been disclosed). (As depicted in Fig. 8).

Boundary conditions. For modal analysis we fixed Z-axis rotation and translation and stiff behavior at both ends, displacements are employed as a constraint for modal analysis. Two displacements at the level of bearing A and B with fixed Z-axis rotation and translation and rigid behavior at both ends are utilized as a restriction for harmonic response analysis (see Figs. 9 and 10). The unbalanced forces, stresses, phase angles, and deformations are measured at the first natural frequencies because the initial resonance possibility is at the first mode.

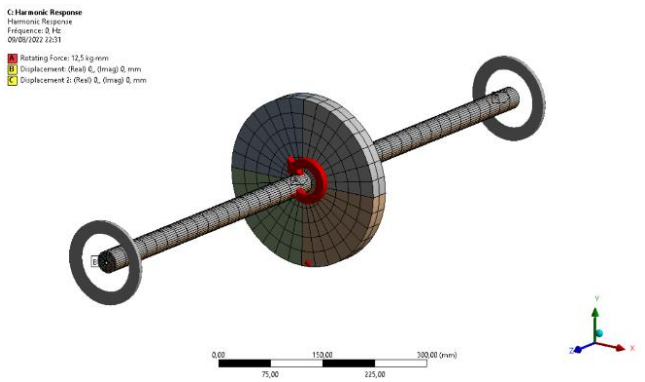

Fig. 10. Boundary conditions of the Jeffcott rotor model: harmonis response analysis

Results and Discussion

Modal Analysis. The following Tables 2-5 indicate the natural frequencies of the Jeffcott rotor for four materials and for ten different modes. In Tables 2-5, we notice that the natural frequencies in the almost four materials are similar and increase progressively, 0 Hz in the first mode, 265.27 Hz in the fifth mode, 652.73 Hz in the tenth mode, 1596.2 Hz in the fifteenth

mode, 2685 Hz in twentieth mode. In this case, we will simply extract the results in the last ten frequencies only and comment on them.

For JIS-S45C steel material. The maximum deformation for the material *(JIS-S45C steel material)* and varies from 13.948 mm at 1st mode, 18.134 mm at 2nd mode, 12.989 mm at 3rd mode, 18.045 mm at 4th mode, 27.928 mm at 5th mode, 27.887 mm at 6th mode, 15.294 mm at 7th mode, 20.07 mm at 8th mode, 19.364 mm at 9th mode, 15.293 mm at 10th mode as shown in Fig. 11.

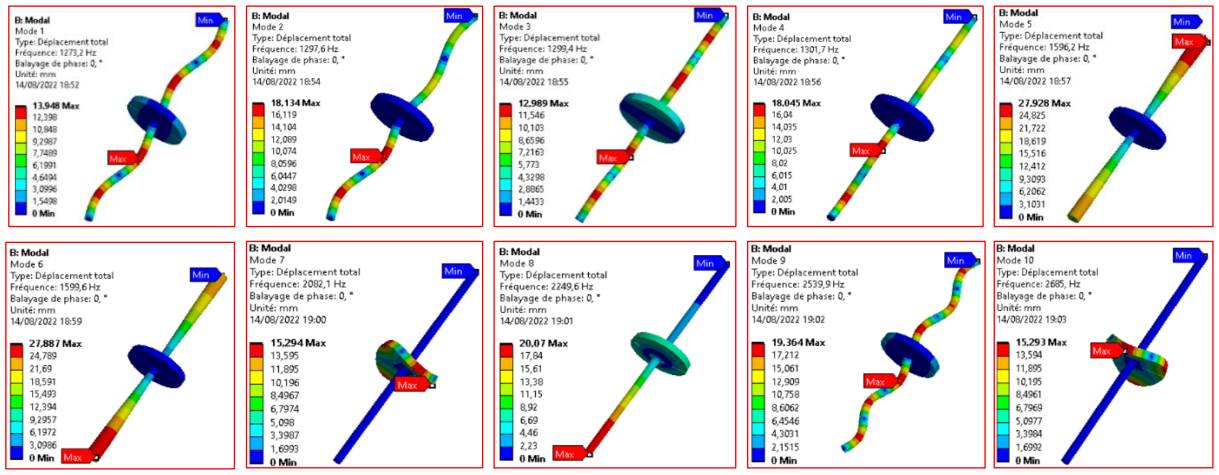

(a)

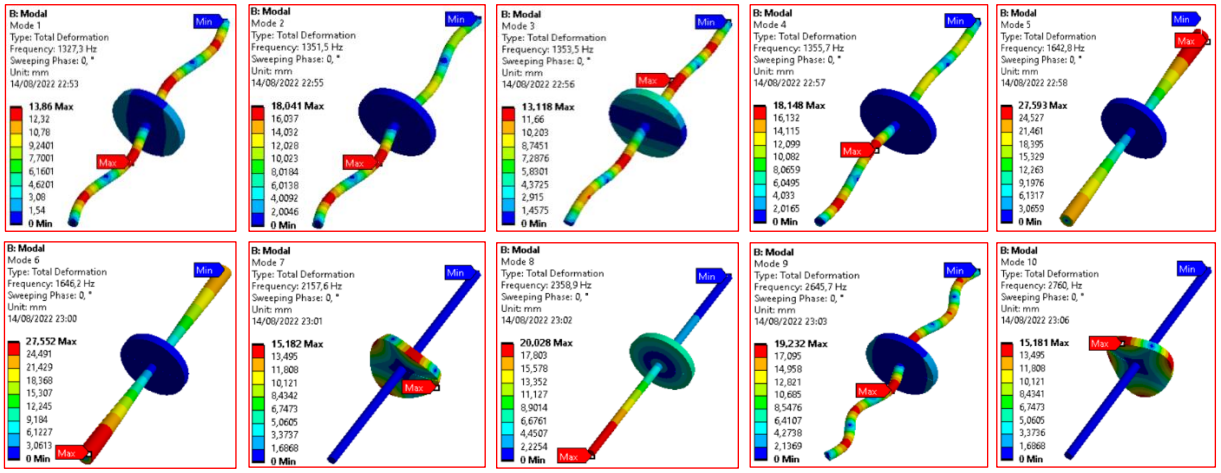

(b)

Fig. 11. Different modes shapes with two materials: JIS-S45C steel material (a), 38CrMoAl steel material (b)

For 38CrMoAl steel material. The maximum deformation for the material *(38CrMoAl steel material)* and varies from 13.86 mm at 1st mode, 18.041 mm at 2nd mode, 13.118 mm at 3rd mode, 18.148 mm at 4th mode, 27.593 mm at 5th mode, 27.552 mm at 6th mode, 15.182 mm at 7th mode, 20.028 mm at 8th mode, 19.232 mm at 9th mode, 15.181 mm at 10th mode as shown in Fig. 11. The natural frequencies and several modes of two materials are shown in the above Tables 2, 3 when the speed varies from 0 to10000 rpm.

For JIS-S45C steel material. The resonance occurrence possibilities are found from the whirl map diagram in the first 3 modes. 1784.2 rpm in a backward whirl at a natural frequency of 29.72 Hz, 1784.9 rpm in a forward whirl at a natural frequency of 29.765 Hz, 8147.7 rpm in the backward whirl at a natural frequency of 123.55 Hz as shown in Table. 2.

Table. 2. Whirl map Campbell Diagram of JIS S45C steel material

Mode	Whirl Direction	Mode Stability	Critical Speed	0, rpm	10000 rpm
1	UNDETERMINED	UNSTABLE	0, rpm	0, Hz	0, Hz
2	BW	STABLE	1784,2 rpm	29,74 Hz	29,72 Hz
3	FW	STABLE	1784,9 rpm	29,745 Hz	29,765 Hz
4	BW	STABLE	8147,7 rpm	189,64 Hz	123,55 Hz
5	FW	STABLE	0, rpm	189,66 Hz	265,27 Hz
6	BW	STABLE	0, rpm	425,59 Hz	425,14 Hz
7	FW	STABLE	0, rpm	425,79 Hz	426,24 Hz
8	BW	STABLE	0, rpm	512,33 Hz	463,43 Hz
9	FW	STABLE	0, rpm	512,69 Hz	619,19 Hz
10	FW	STABLE	0, rpm	652,73 Hz	652,73 Hz
11	BW	STABLE	0, rpm	1282,6 Hz	1273,2 Hz
12	BW	STABLE	0, rpm	1284,3 Hz	1297,6 Hz
13	FW	STABLE	0, rpm	1298,9 Hz	1299,4 Hz
14	FW	STABLE	0, rpm	1300,5 Hz	1301,7 Hz
15	BW	STABLE	0, rpm	1596,2 Hz	1596,2 Hz
16	BW	STABLE	0, rpm	1599,6 Hz	1599,6 Hz
17	BW	STABLE	0, rpm	2249,6 Hz	2082,1 Hz
18	FW	STABLE	0, rpm	2364,1 Hz	2249,6 Hz
19	BW	STABLE	0, rpm	2364,8 Hz	2539,9 Hz
20	FW	STABLE	0, rpm	2539,6 Hz	2685, Hz

For 38CrMoAl steel material. The resonance occurrence possibilities are found from the whirl map diagram in the first 3 modes. 1858.7 rpm in a backward whirl at a natural frequency of 30.962 Hz, 1859.4 rpm in a forward whirl at a natural frequency of 31.007 Hz, 8468.1 rpm in the backward whirl at a natural frequency of 130.94 Hz as shown in Table. 3.

Table. 3. Whirl map Campbell Diagram of 38CrMoAl steel material

Mode	Whirl Direction	Mode Stability	Critical Speed	0, rpm	10000 rpm
1	UNDETERMINED	STABLE	0, rpm	3,5879e-004 Hz	3,5879e-004 Hz
2	BW	STABLE	1858,7 rpm	30,982 Hz	30,962 Hz
3	FW	STABLE	1859,4 rpm	30,987 Hz	31,007 Hz
4	BW	STABLE	8468,1 rpm	197,51 Hz	130,94 Hz
5	FW	STABLE	0, rpm	197,53 Hz	273,46 Hz
6	BW	STABLE	0, rpm	443,38 Hz	442,93 Hz
7	FW	STABLE	0, rpm	443,59 Hz	444,04 Hz
8	BW	STABLE	0, rpm	534,24 Hz	484,63 Hz
9	FW	STABLE	0, rpm	534,62 Hz	639,49 Hz
10	FW	STABLE	0, rpm	680,55 Hz	680,55 Hz
11	BW	STABLE	0, rpm	1336,7 Hz	1327,3 Hz
12	BW	STABLE	0, rpm	1338,5 Hz	1351,5 Hz
13	FW	STABLE	0, rpm	1352,8 Hz	1353,5 Hz
14	FW	STABLE	0, rpm	1354,5 Hz	1355,7 Hz
15	BW	STABLE	0, rpm	1642,8 Hz	1642,8 Hz
16	BW	STABLE	0, rpm	1646,2 Hz	1646,2 Hz
17	BW	STABLE	0, rpm	2358,9 Hz	2157,6 Hz
18	FW	STABLE	0, rpm	2439,9 Hz	2358,9 Hz
19	BW	STABLE	0, rpm	2440,7 Hz	2645,7 Hz
20	FW	STABLE	0, rpm	2645,4 Hz	2760, Hz

Figure 12 shows the Whirl map diagram/Campbell diagram for four materials with their critical speeds is shown above. The Campbell diagram, also known as whirl speed map or a frequency interface diagram, of a simple rotor system. On the other hand, the rotor system is made by the two materials (JIS-S45C steel material, 38CrMoAl steel material), The occurrence

possibilities of operating well at response speed are found from the wirl map diagram in the 14 following modes (265.27, 425.14, 426.24, 463.43, 619.19, 652.73, 1273.2, 1297.6, 1299.4, 1301.7, 1596.2, 1599.6, 2082.1, 2249.6, 2539.9, 2685 Hz), (273.46, 442.93, 444.04, 484.63, 639.49, 680.55, 1327.3, 1351.5, 1353.5,1355.7, 1642.8, 1646.2, 2157.6, 2358.9, 2645.7, 2760 Hz) for 38CrMoAl steel material, as shown in the Table. 3. For the two materials *(JIS-S45C steel material, 38CrMoAl steel material)*, the critical velocity occurrence possibilities are found from the wirl map diagram in the first 3 modes (29.72, 29.765, 123, 55Hz), (30.962, 31.007, 130.94Hz) as shown in Tables 2 and 3.

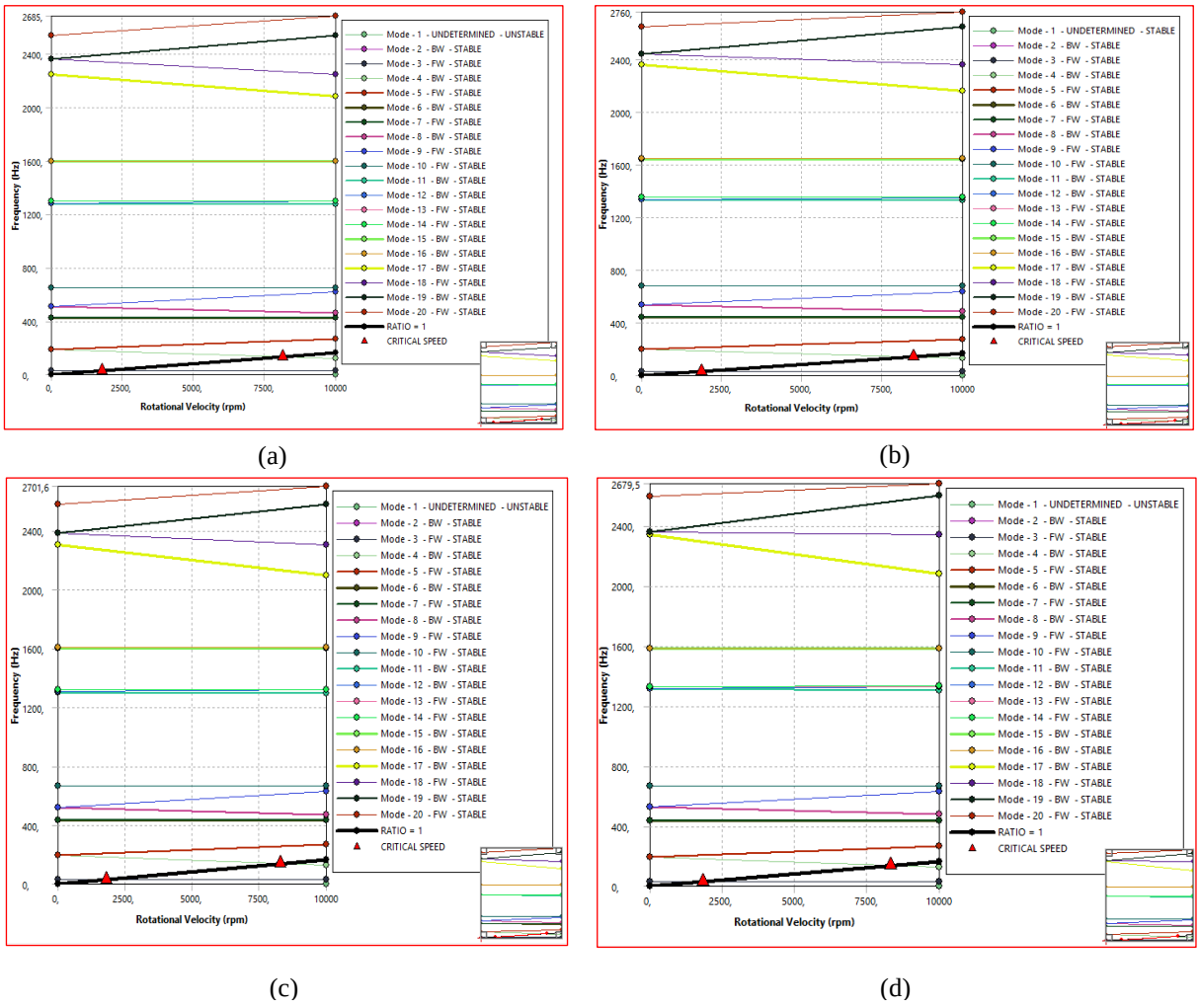

Fig. 12. Whirl map Campbell diagram with four materials: (a) JIS-S45C steel material; (b) 38CrMoAl steel material: (c) structural steel material; (d) titanium alloy (Ti-6AL-4V) material

For structure steel material: The maximum total deformation for this type of material is almost larger at each mode and varies from 437.97 mm at 1st mode, 557.88 mm at 2nd mode, 446.39 mm at 3rd mode, 585.74 mm at 4th mode, 872.55 mm at 5th mode, 871.26 mm at 6th mode, 480.07 mm at 7th mode, 633.35 mm at 8th mode, 608.17 mm at 9th mode, 480.07 mm at 10th mode. The natural frequencies and several modes of this material are shown in Table 4 and Fig. 13 when the speed varies from 0 rpm to 10,000 rpm.

The resonance occurrence possibilities are found from the whirl map diagram in the first 3 modes. 1813.9rpm in backward whirl at natural frequency of 30.2015 Hz, 1814.6 rpm in forward whirl at natural frequency of 30.261 Hz, 8275.9 rpm in the backward whirl at natural frequency of 126.51 Hz as shown in Table. 4. On the other hand, the rotor system is made by the materials *(structure steel material)*. The occurrence possibilities of operating well at

response speed are found from the wirl map diagram in the 14 following modes (268.47, 432.25, 433.35, 472.16, 627.5, 664.15, 1295.1, 1318.9, 1321.4, 1323.1, 1603.2, 1606.5, 2099.3, 2302, 2582, 2701.6 Hz), as shown in the Table 4.

Table. 4. Whirl map Campbell diagram of Structural Steel material.

Mode	Whirl Direction	Mode Stability	Critical Speed	0, rpm	10000 rpm
1	UNDETERMINED	UNSTABLE	0, rpm	0, Hz	0, Hz
2	BW	STABLE	1813,9 rpm	30,236 Hz	30,215 Hz
3	FW	STABLE	1814,6 rpm	30,24 Hz	30,261 Hz
4	BW	STABLE	8275,9 rpm	192,75 Hz	126,51 Hz
5	FW	STABLE	0, rpm	192,77 Hz	268,47 Hz
6	BW	STABLE	0, rpm	432,69 Hz	432,25 Hz
7	FW	STABLE	0, rpm	432,9 Hz	433,35 Hz
8	BW	STABLE	0, rpm	521,37 Hz	472,16 Hz
9	FW	STABLE	0, rpm	521,74 Hz	627,5 Hz
10	FW	STABLE	0, rpm	664,15 Hz	664,15 Hz
11	BW	STABLE	0, rpm	1304,5 Hz	1295,1 Hz
12	BW	STABLE	0, rpm	1306,2 Hz	1318,9 Hz
13	FW	STABLE	0, rpm	1320,2 Hz	1321,4 Hz
14	FW	STABLE	0, rpm	1321,9 Hz	1323,1 Hz
15	BW	STABLE	0, rpm	1603,2 Hz	1603,2 Hz
16	BW	STABLE	0, rpm	1606,5 Hz	1606,5 Hz
17	BW	STABLE	0, rpm	2302, Hz	2099,3 Hz
18	FW	STABLE	0, rpm	2381,1 Hz	2302, Hz
19	BW	STABLE	0, rpm	2381,8 Hz	2582, Hz
20	FW	STABLE	0, rpm	2581,6 Hz	2701,6 Hz

Table. 5. Whirl map Campbell diagram of titanium alloy (Ti-6AL-4V) material.

5	Whirl Direction	Mode Stability	Critical Speed	0, rpm	10000 rpm
1	UNDETERMINED	UNSTABLE	0, rpm	0, Hz	0, Hz
2	BW	STABLE	1824,8 rpm	30,417 Hz	30,397 Hz
3	FW	STABLE	1825,5 rpm	30,422 Hz	30,442 Hz
4	BW	STABLE	8323,9 rpm	193,82 Hz	127,64 Hz
5	FW	STABLE	0, rpm	193,83 Hz	269,47 Hz
6	BW	STABLE	0, rpm	435,35 Hz	434,9 Hz
7	FW	STABLE	0, rpm	435,56 Hz	436,01 Hz
8	BW	STABLE	0, rpm	525,48 Hz	476,11 Hz
9	FW	STABLE	0, rpm	525,87 Hz	631,18 Hz
10	FW	STABLE	0, rpm	669,2 Hz	669,2 Hz
11	BW	STABLE	0, rpm	1313,6 Hz	1304,1 Hz
12	BW	STABLE	0, rpm	1315,4 Hz	1326,5 Hz
13	FW	STABLE	0, rpm	1327,7 Hz	1330,3 Hz
14	FW	STABLE	0, rpm	1329,4 Hz	1330,9 Hz
15	BW	STABLE	0, rpm	1581,2 Hz	1581,2 Hz
16	BW	STABLE	0, rpm	1584,5 Hz	1584,5 Hz
17	BW	STABLE	0, rpm	2342,6 Hz	2078,1 Hz
18	FW	STABLE	0, rpm	2359,4 Hz	2342,6 Hz
19	BW	STABLE	0, rpm	2360,1 Hz	2597,7 Hz
20	FW	STABLE	0, rpm	2597,4 Hz	2679,5 Hz

For titanium alloy (Ti-6AL-4V) material. The maximum total deformation for this type of material is almost larger at each mode and varies from 18.512 mm at 1st mode, 22.787 mm at 2nd mode, 26.196 mm at 3rd mode, 28.491 mm at 4th mode, 36.515 mm at 5th mode, 36.46 mm at 6th mode, 20.284 mm at 7th mode, 27.021 mm at 8th mode, 25.738 mm at 9th mode, 20.286 mm at 10th mode. The natural frequencies and several modes of this material are shown in Table 5 and Fig. 13 above when the speed varies from 0 rpm to 10,000 rpm.

The resonance occurrence possibilities are found from the whirl map diagram in the first 3 modes. 1824.8 rpm in backward whirl at natural frequency of 30.397 Hz, 1825.5 rpm in forward whirl at natural frequency of 30.442 Hz, 8323.9 rpm in the backward whirl at natural frequency of 127.64 Hz as shown in Table. 5.

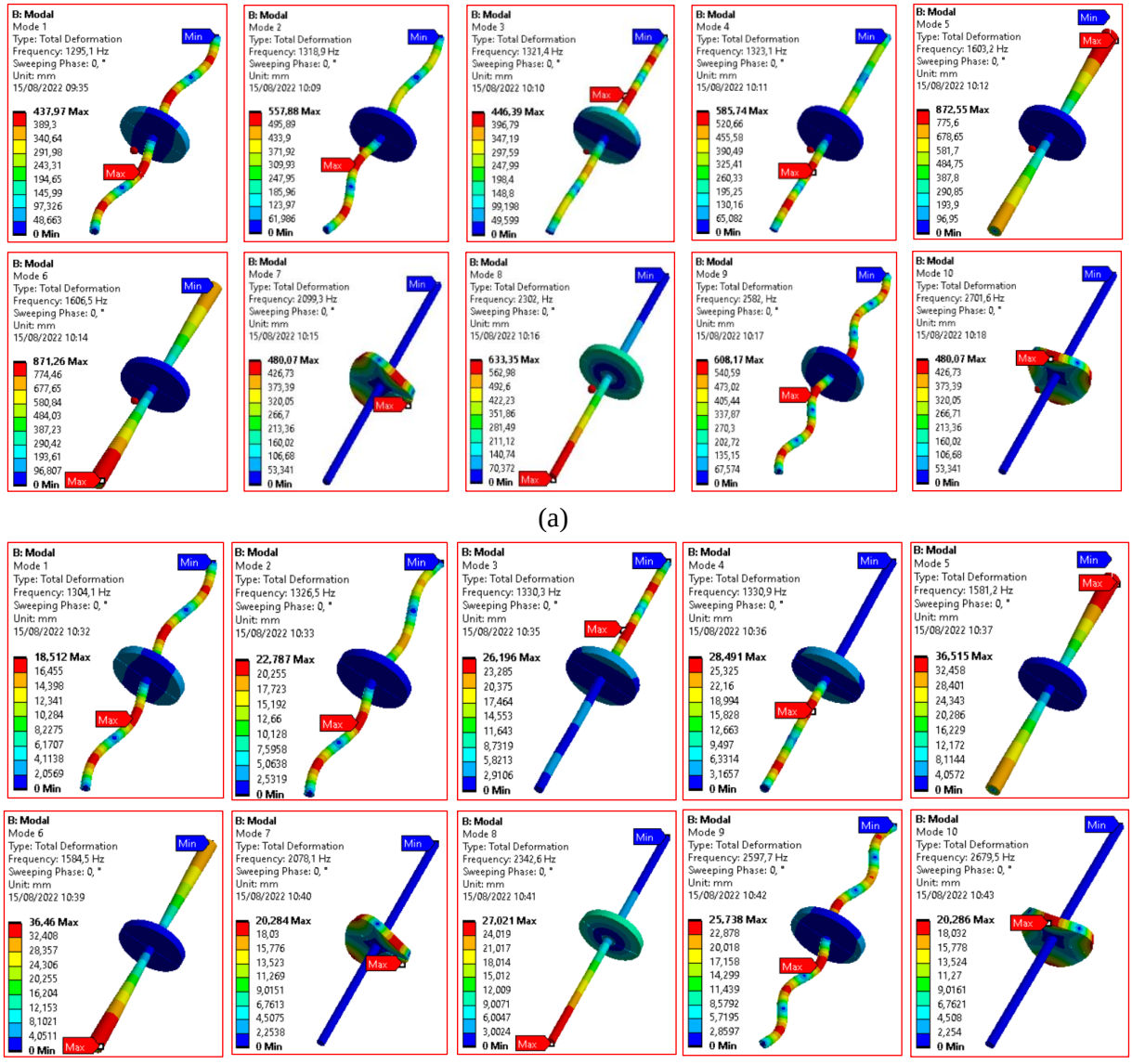

Fig. 13. Different modes shapes with two materials: (a) structural steel material, (b) titanium alloy (Ti-6AL-4V) material

On the other hand, the rotor system is made by the materials *(titanium alloy (Ti-6AL-4V))*. The occurrence possibilities of operating well at response speed are found from the wirl map diagram in the 14 following modes (269.47, 434.9, 436.01, 476.11, 631.18, 669.2, 1304.1, 1326.5, 1330.3, 1330.9, 1581.2, 1584.5, 2078.1, 2342.6, 2597.7, 2679.5 Hz), as shown in the Table 5.

Harmonic response analysis. Analysis of the harmonic response of a rotor allows us to determine the deformations, Von Mises stresses, principal stresses, maximum shear stresses and phase angle effect due to balanced and unbalanced forces acting on the system rotor-shaft.

Stress severity for Jeffcott rotor. The following data represents results of the harmonic response analysis of the Jeffcott rotor for the four different materials based on the stress severity.

Figure 14 explains the stresses severity due to the unbalance force for four materials. When the 0.1 kg of unbalanced mass added on the disk with the increasing, the frequencies from 270 to 2700 Hz with step size 100 Hz.

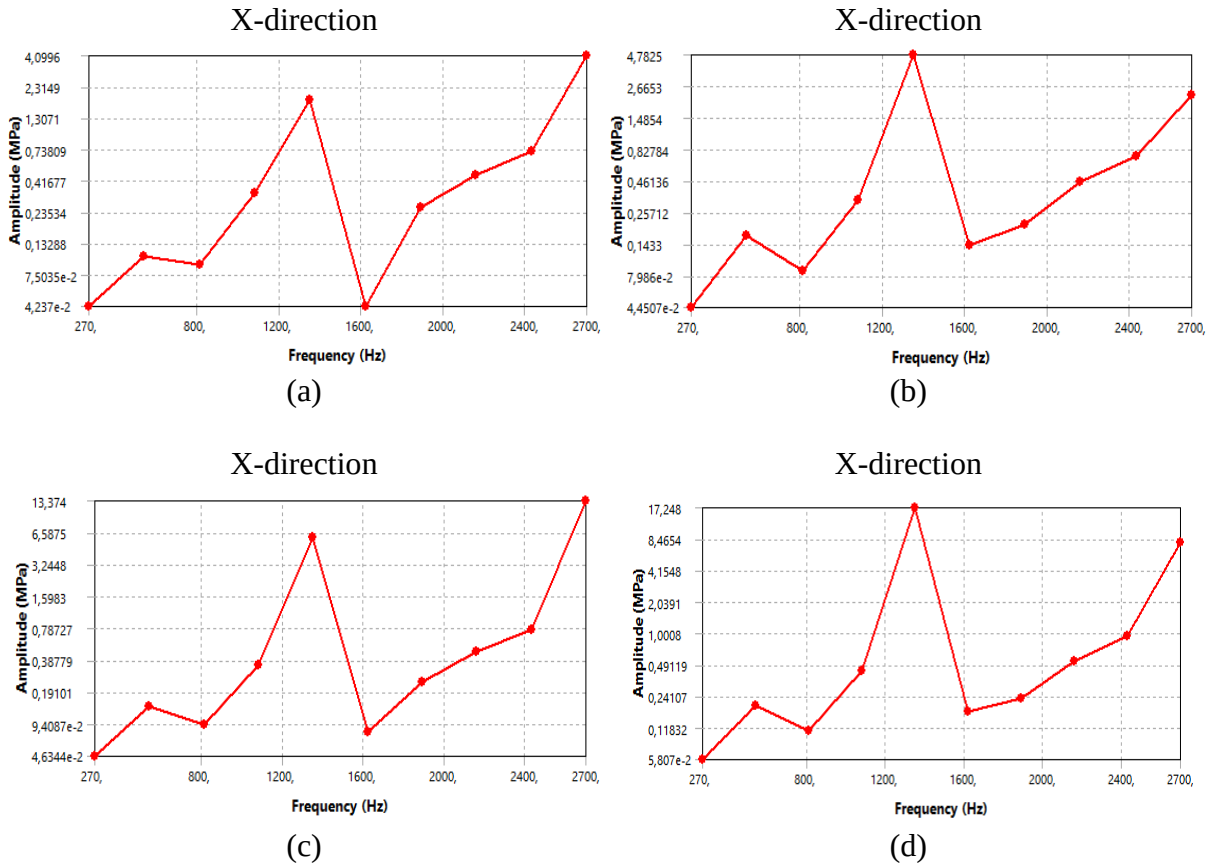

Fig. 14. Stress severity for Jeffcott rotor with 4 varieties of materials due to the unbalance forces: (a) JIS-S45C; (b) 38CrMoAl; (c) structural steel; (d) Ti-6AL-4V

For a steel material of JIS-S45C. When 0.1 kg of unbalance is added to the disk with the increase in frequencies from 270 to 2700 Hz with a step of 100 Hz, the maximum amplitude of normal stress total along X varies from 4.237E-2 MPa at 270 Hz, 1.805 MPa at 1350 Hz and 4.0996 MPa at 2700 Hz a shown in Fig. 14.

For a steel material of 38CrMoAl. When 0.1 kg of unbalance is added to the disk with the increase in frequencies from 270 to 2700 Hz with a step of 100 Hz, the maximum amplitude of normal stress total along X varies from 4.4507E-2 MPa at 270 Hz, 4.7825 MPa at 1350 Hz and 2.6653 MPa at 2700 Hz this mentioned in Fig. 14.

For a material of structural steel. When 0.1 kg of unbalance is added to the disk with the increase in frequencies from 270 to 2700 Hz with a step of 100 Hz, the maximum amplitude of normal stress total along X varies from 4.6344E-2 MPa at 270 Hz, 6.5875 MPa at 1350 Hz and 13.374 MPa at 2700 Hz a shown in Fig. 14.

For a material of titanium alloy (Ti-6AL-4V). When 0.1 kg of unbalance is added to the disk with the increase in frequencies from 270 to 2700 Hz with a step of 100 Hz, the maximum amplitude of normal stress total along X varies from 5.807E-2 MPa at 270 Hz, 17.248 MPa at 1350 Hz and 8.4654 MPa at 2700 Hz this mentioned in Fig. 14.

For a steel material of JIS-S45C. When 0.1 kg of unbalance is added to the disk with the increase in frequencies from 270 to 2700 Hz with a step of 100 Hz, the maximum amplitude of normal stress total along Y varies from 3.4435E-2 MPa at 270 Hz, 3.02MPa at 1350 Hz and 20.648 MPa at 2700 Hz a shown in Fig. 15.

For a steel material of 38CrMoAl. When 0.1 kg of unbalance is added to the disk with the increase in frequencies from 270 to 2700 Hz with a step of 100 Hz, the maximum amplitude of normal stress total along Y varies from 3.618E-2 MPa at 270 Hz, 7.3703 MPa at 1350 Hz and 7.3703 MPa at 2700 Hz this mentioned in Fig. 15.

For a material of structural steel. When 0.1 kg of unbalance is added to the disk with the increase in frequencies from 270 to 2700 Hz with a step of 100 Hz, the maximum amplitude of normal stress total along Y varies from 3.7946E-2 MPa at 270 Hz, 8.9688 MPa at 1350 Hz and 55.453 MPa at 2700 Hz a shown in Fig. 15.

For a material of titanium alloy (Ti-6AL-4V). When 0.1 kg of unbalance is added to the disk with the increase in frequencies from 270 to 2700 Hz with a step of 100 Hz, the maximum amplitude of normal stress total along Y varies from 4.8007E-2 MPa at 270 Hz, 18.335 MPa at 1350 Hz and 25.171 at 2700 Hz this mentioned in Fig. 15.

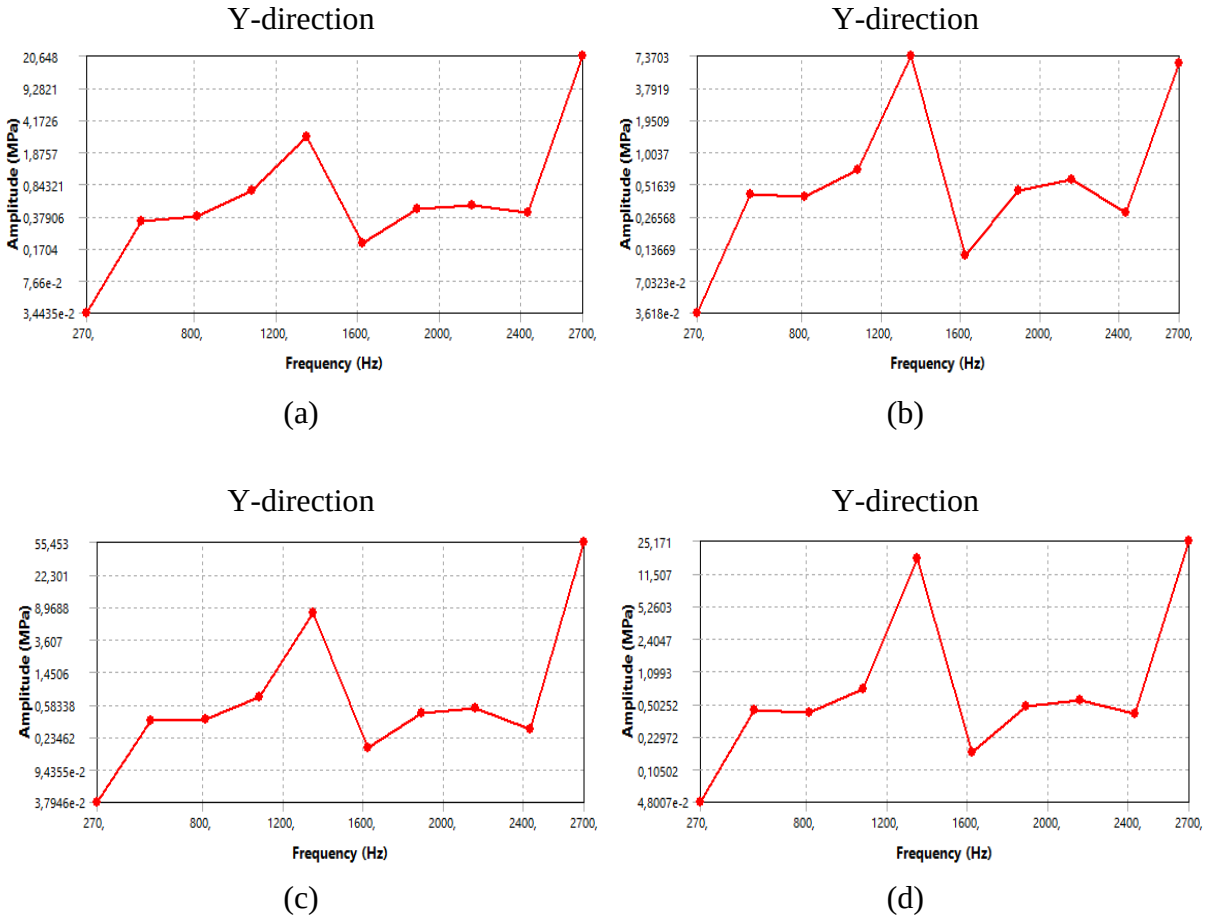

Fig. 15. Stress severity for Jeffcott rotor with 4 varieties of materials due to the unbalance forces: (a) JIS-S45C; (b) 38CrMoAl; (c) structural steel; (d) Ti-6AL-4V

For a steel material of JIS-S45C. When 0.1 kg of unbalance is added to the disk with the increase in frequencies from 270 to 2700 Hz with a step of 100 Hz, the maximum amplitude of normal stress total along Y varies from 0.3983 MPa at 270 Hz, 23.773 MPa at 1350 Hz and 46.995 MPa at 2700 Hz a shown in Fig. 16.

For a steel material of 38CrMoAl. When 0.1 kg of unbalance is added to the disk with the increase in frequencies from 270 to 2700 Hz with a step of 100 Hz, the maximum amplitude of normal stress total along Y varies from 0.3027 MPa at 270 Hz, 39.891 MPa at 1350 Hz and 21.672 MPa at 2700 Hz this mentioned in Fig. 16.

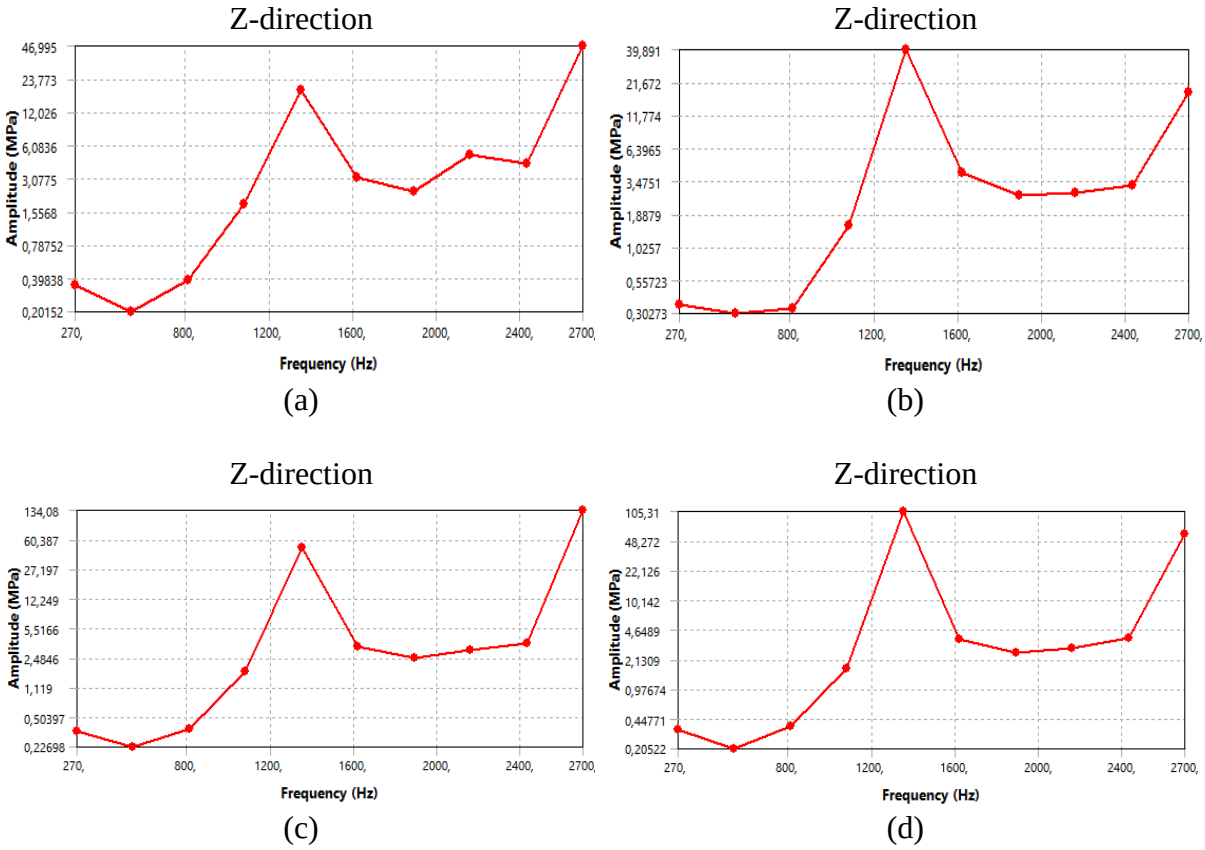

Fig. 16. Stress severity for Jeffcott rotor with 4 varieties of materials due to the unbalance forces: (a) JIS-S45C, (b) 38CrMoAl, (c) structural steel, and (d) Ti-6AL-4V

For a material of Structural Steel When 0.1 kg of unbalance is added to the disk with the increase in frequencies from 270 to 2700 Hz with a step of 100 Hz, the maximum amplitude of normal stress total along Y varies from 0.3 MPa at 270 Hz, 60.387 MPa at 1350 Hz and 134.08 MPa at 2700 Hz a shown in Fig. 16.

For a material of titanium alloy (Ti-6AL-4V). When 0.1 kg of unbalance is added to the disk with the increase in frequencies from 270 to 2700 Hz with a step of 100 Hz, the maximum amplitude of normal stress total along Y varies from 0.31 MPa at 270 Hz, 105.31 MPa at 1350 Hz and 48.272 at 2700 Hz this mentioned in Fig. 12.

Deformation severity for Jeffcott rotor. Figure 13 explains the deformation severity due to the unbalance force for four materials. When the 0.1 kg of unbalanced mass added on the disk with the increasing, the frequencies from 270 to 2700 Hz with step size 100 Hz.

For a steel material of JIS-S45C. When 0.1 kg of unbalance is added to the disk with the increase in frequencies from 270 to 2700 Hz with a step of 100 Hz, the maximum amplitude of deformation total along X varies from 0.83667 mm at 270 Hz, 0.1374 mm at 1350 Hz and 1.5277 mm at 2700 Hz a shown in Fig. 17.

For a steel material of 38CrMoAl. When 0.1 kg of unbalance is added to the disk with the increase in frequencies from 270 to 2700 Hz with a step of 100 Hz, the maximum amplitude of deformation total along X varies from 0.7506 mm at 270 Hz, 0.7506 mm at 1350 Hz and 1.0275 mm at 2700 Hz a shown in Fig. 17.

For a material of structural steel. When 0.1 kg of unbalance is added to the disk with the increase in frequencies from 270 to 2700 Hz with a step of 100 Hz, the maximum amplitude of deformation total along X varies from 0.70512 mm at 270 Hz, 0.17663 mm at 1350 Hz and 5.6242 mm at 2700 Hz a shown in Fig. 17.

For a material of titanium alloy (Ti-6AL-4V). When 0.1 kg of unbalance is added to the disk with the increase in frequencies from 270 to 2700 Hz with a step of 100 Hz, the maximum amplitude of deformation total along X varies from 1.27589 mm at 270 Hz, 1.27589 mm at 1350 Hz and 4.7221 mm at 2700 Hz a shown in Fig. 17.

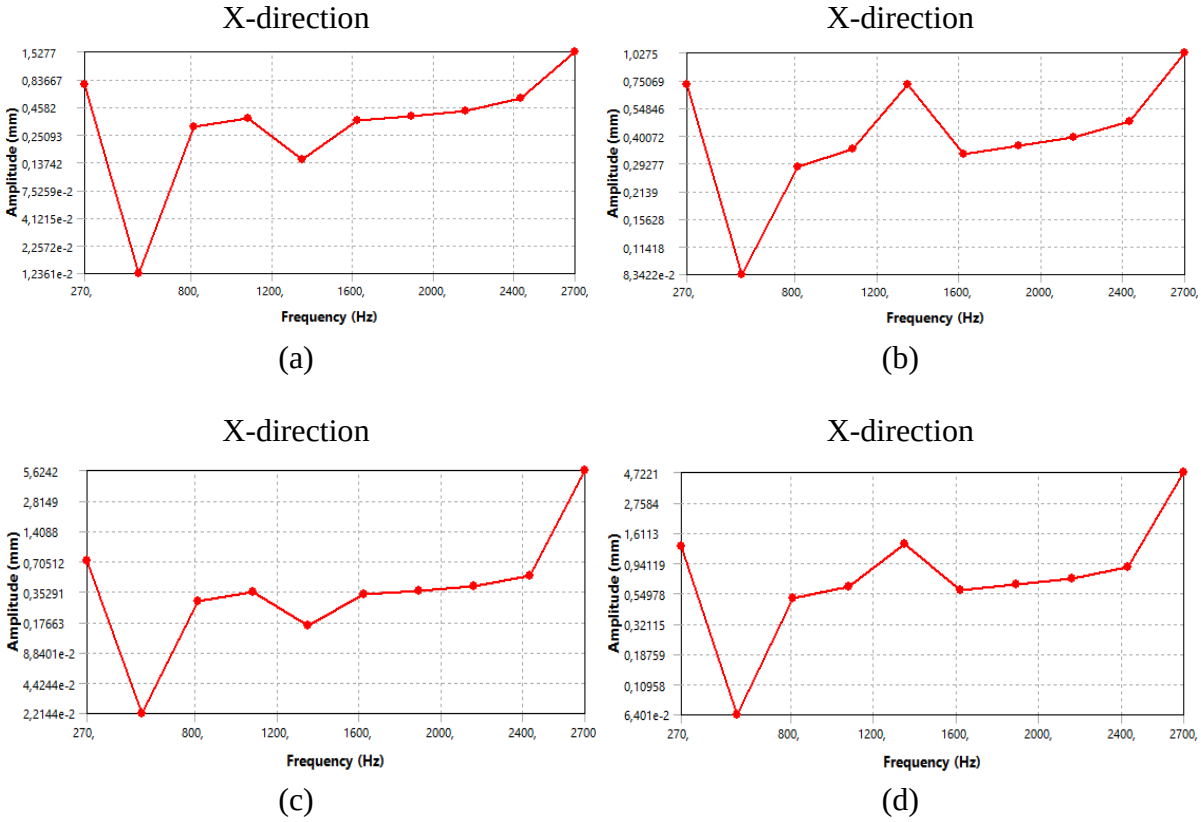

Fig. 17. Deformation severity for Jeffcott rotor with 4 varieties of materials due to the unbalance forces. (a) JIS-S45C; (b) 38CrMoAl; (c) structural steel; (d) Ti-6AL-4V

For a steel material of JIS-S45C. When 0.1 kg of unbalance is added to the disk with the increase in frequencies from 270 to 2700 Hz with a step of 100 Hz, the maximum amplitude of deformation total along Y varies from 0.84969 mm at 270 Hz, 0.1356 mm at 1350 Hz and 1.5664 mm at 2700 Hz a shown in Fig. 18.

For a steel material of 38CrMoAl. When 0.1 kg of unbalance is added to the disk with the increase in frequencies from 270 to 2700 Hz with a step of 100 Hz, the maximum amplitude of deformation total along Y varies from 0.69327 mm at 270 Hz, 0.80392 mm at 1350 Hz and 1.1093 mm at 2700 Hz a shown in Fig. 18.

For a material of Structural Steel. When 0.1 kg of unbalance is added to the disk with the increase in frequencies from 270 to 2700 Hz with a step of 100 Hz, the maximum amplitude of deformation total along Y varies from 0.72833 mm at 270 Hz, 0.18248 mm at 1350 Hz and 5.8078 mm at 2700 Hz a shown in Fig. 18.

For a material of titanium alloy (Ti-6AL-4V). When 0.1 kg of unbalance is added to the disk with the increase in frequencies from 270 to 2700 Hz with a step of 100 Hz, the maximum amplitude of deformation total along Y varies from 1.31794 mm at 270 Hz, 1.31794 mm at 1350 Hz and 4.897 mm at 2700 Hz a shown in Fig. 18.

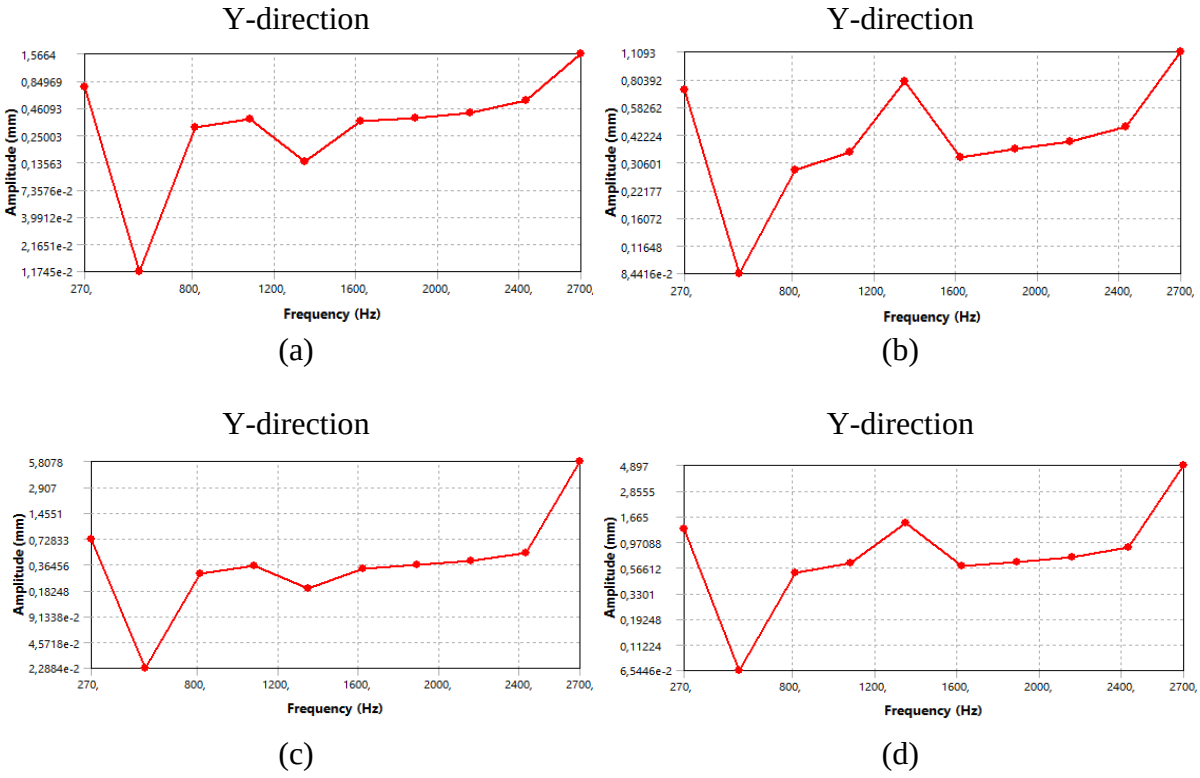

Fig. 18. Deformation severity for Jeffcott rotor with 4 varieties of materials due to the unbalance forces: (a) JIS-S45C, (b) 38CrMoAl, (c) structural steel, (d) Ti-6AL-4V

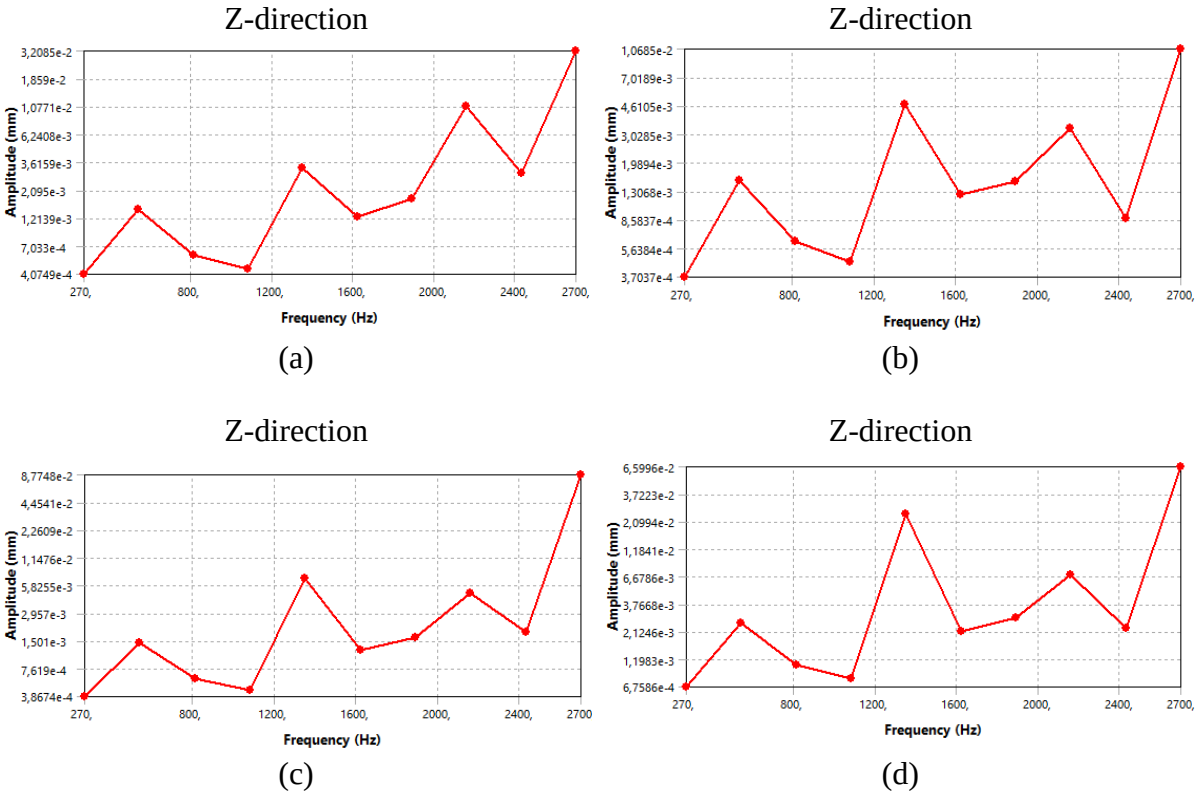

Fig. 19. Deformation severity for Jeffcott rotor with 3 varieties of materials due to the unbalance forces

For a steel material of JIS-S45C. When 0.1 kg of unbalance is added to the disk with the increase in frequencies from 270 to 2700 Hz with a step of 100 Hz, the maximum amplitude of deformation total along Z varies from 4.0779E-4 mm at 270 Hz, 3.6159E-3 mm at 1350 Hz and 3.2085E-2 mm mm at 2700 Hz a shown in Fig. 19.

For a steel material of 38CrMoAl. When 0.1 kg of unbalance is added to the disk with the increase in frequencies from 270 to 2700 Hz with a step of 100 Hz, the maximum amplitude of deformation total along Z varies from 3.7037E-4 mm at 270 Hz, 4.6105E-3 mm at 1350 Hz and 1.0685E-2 mm mm at 2700 Hz a shown in Fig. 19.

For a material of structural Steel. When 0.1 kg of unbalance is added to the disk with the increase in frequencies from 270 to 2700 Hz with a step of 100 Hz, the maximum amplitude of deformation total along Z varies from 3.8674E-4 mm at 270 Hz, 5.8255E-3 mm at 1350 Hz and 8.7748E-2 mm at 2700 Hz a shown in Fig. 19.

For a material of Titanium Alloy (Ti-6AL-4V). When 0.1 kg of unbalance is added to the disk with the increase in frequencies from 270 to 2700 Hz with a step of 100 Hz, the maximum amplitude of deformation total along Z varies from 6.7586E-4 mm at 270 Hz, 2.0994E-2 mm at 1350 Hz and 6.5996E-2 mm mm at 2700 Hz a shown in Fig. 19.

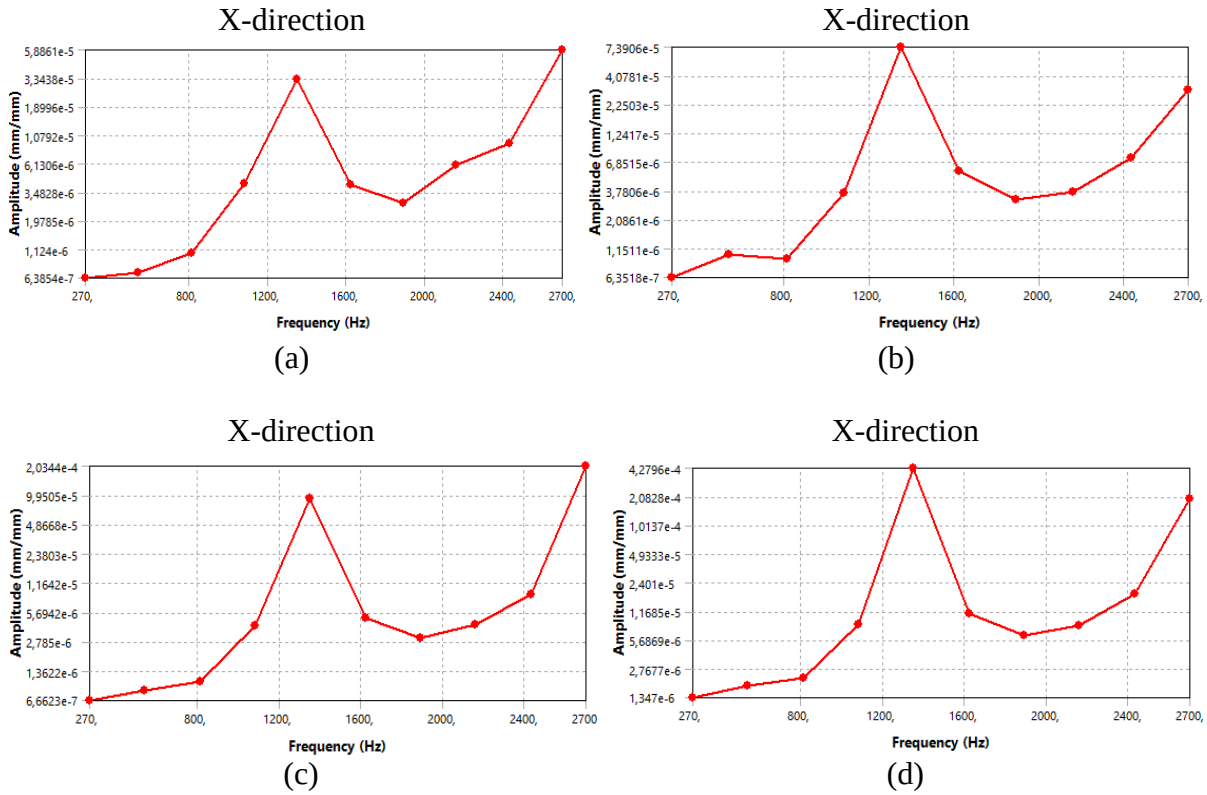

Fig. 20. Normal elastic strain severity for Jeffcott rotor with 4 varieties of materials due to the unbalance forces. (a) JIS-S45C; (b) 38CrMoAl; (c) structural steel; (d) Ti-6AL-4V

Normal elastic strain severity for Jeffcott rotor. Figure 20 explains normal elastic strain severity due to the unbalance force for four materials. When the 0.1 kg of unbalanced mass added on the disk with the increasing, the frequencies from 270 to 2700 Hz with step size 100 Hz.

For a steel material of JIS-S45C. When 0.1 kg of unbalance is added to the disk with the increase in frequencies from 270 to 2700 Hz with a step of 100 Hz, the maximum amplitude of normal elastic strain along X varies from 6.3854E-7 mm at 270 Hz, 3.3438E-5 mm at 1350 Hz and 5.8861E-5 mm at 2700 Hz a shown in Fig. 20.

For a steel material of 38CrMoAl. When 0.1 kg of unbalance is added to the disk with the increase in frequencies from 270 to 2700 Hz with a step of 100 Hz, the maximum amplitude of normal elastic strain along X varies from 6.3518E-7 mm at 270 Hz, 7.3906E-5 mm at 1350 Hz and 3.16E-5 mm at 2700 Hz a shown in Fig. 20.

For a material of structural steel. When 0.1 kg of unbalance is added to the disk with the increase in frequencies from 270 to 2700 Hz with a step of 100 Hz, the maximum amplitude of normal elastic strain along X varies from 6.6623E-7 mm at 270 Hz, 9.9505E-5 mm at 1350 Hz and 2.0344E-1 mm at 2700 Hz a shown in Fig. 20.

For a material of titanium alloy (Ti-6AL-4V). When 0.1 kg of unbalance is added to the disk with the increase in frequencies from 270 to 2700 Hz with a step of 100 Hz, the maximum amplitude of normal elastic strain along X varies from 1.347E-6 mm at 270 Hz, 4.2796E-4 mm at 1350 Hz and 2.0828E-4 mm mm at 2700 Hz a shown in Fig. 20.

For a steel material of JIS-S45C. When 0.1 kg of unbalance is added to the disk with the increase in frequencies from 270 to 2700 Hz with a step of 100 Hz, the maximum amplitude of normal elastic strain along Y varies from 6.3169E-7 mm at 270 Hz, 9.7506E-6 mm at 1350 Hz and 1.5051E-4 mm at 2700 Hz a shown in Fig. 21.

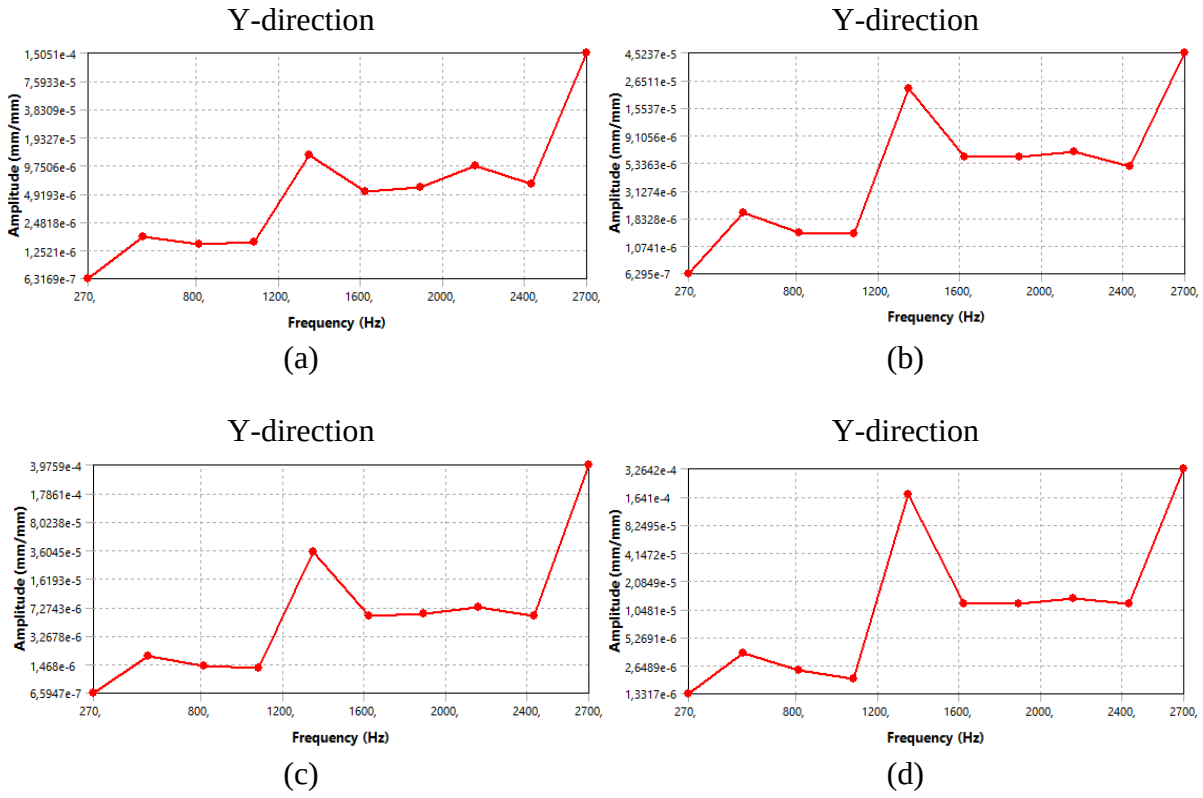

Fig. 21. Normal elastic strain severity for Jeffcott rotor with 4 varieties of materials due to the unbalance forces. (a) JIS-S45C; (b) 38CrMoAl; (c) structural steel; (d) Ti-6AL-4V

For a steel material of 38CrMoAl. When 0.1 kg of unbalance is added to the disk with the increase in frequencies from 270 to 2700 Hz with a step of 100 Hz, the maximum amplitude of normal elastic strain along Y varies from 6.295E-7 mm at 270 Hz, 2.6511E-5 mm at 1350 Hz and 4.5237E-5 mm at 2700 Hz a shown in Fig. 21.

For a material of structural steel. When 0.1 kg of unbalance is added to the disk with the increase in frequencies from 270 to 2700 Hz with a step of 100 Hz, the maximum amplitude of normal elastic strain along Y varies from 6.5947E-7 mm at 270 Hz, 3.6045E-5 mm at 1350 Hz and 3.9757E-4 mm at 2700 Hz a shown in Fig. 21.

For a material of titanium alloy (Ti-6AL-4V). When 0.1 kg of unbalance is added to the disk with the increase in frequencies from 270 to 2700 Hz with a step of 100 Hz, the maximum amplitude of normal elastic strain along Y varies from 1.3317E-6 mm at 270 Hz, 1.641E-4 mm at 1350 Hz and 3.2642E-4 mm at 2700 Hz a shown in Fig. 21.

For a steel material of JIS-S45C. When 0.1 kg of unbalance is added to the disk with the increase in frequencies from 270 Hz to 2700 Hz with a step of 100 Hz, the maximum amplitude of normal elastic strain along Y varies from 2.035E-6mm at 270 Hz, 7.1783E-5mm at 1350 Hz and 2.6707E-4mm mm at 2700 Hz a shown in Fig. 22.

For a steel material of 38CrMoAl. When 0.1 kg of unbalance is added to the disk with the increase in frequencies from 270 to 2700 Hz with a step of 100 Hz, the maximum amplitude of normal elastic strain along Y varies from 2.1237E-6 mm at 270 Hz, 1.8149E-4 mm at 1350 Hz and 9.6134E-5 mm at 2700 Hz a shown in Fig. 22.

For a material of structural steel. When 0.1 kg of unbalance is added to the disk with the increase in frequencies from 270 to 2700 Hz with a step of 100 Hz, the maximum amplitude of normal elastic strain along Y varies from 2.30E-6 mm at 270 Hz, 2.45E-4 mm at 1350 Hz and 7.308E-4 mm at 2700 Hz a shown in Fig. 22.

For a material of titanium alloy (Ti-6AL-4V). When 0.1 kg of unbalance is added to the disk with the increase in frequencies from 270 to 2700 Hz with a step of 100 Hz, the maximum amplitude of normal elastic strain along Y varies from 3.63055E-6mm at 270 Hz, 8.9358E-4 mm at 1350 Hz and 6.59265E-4 mm at 2700 Hz a shown in Fig. 22.

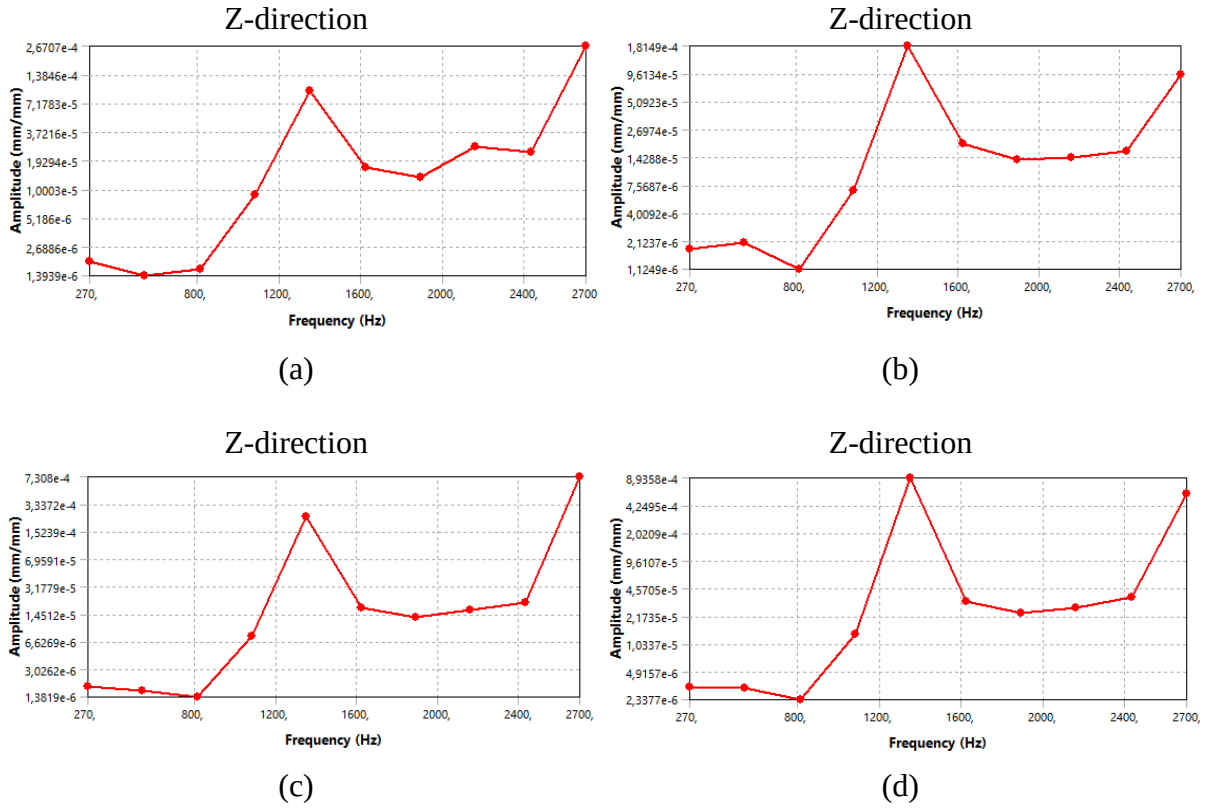

Fig. 22. Normal elastic strain severity for Jeffcott rotor with 3 varieties of materials due to the unbalance forces. (a) JIS-S45C; (b) 38CrMoAl; (c) structural steel; (d) Ti-6AL-4V

Phase angle effect on stress severity for Jeffcott rotor. Ensuing values of the four chosen materials provides the results of the harmonic response analysis for the Jeffcott rotor based on the phase angle effect with respect to the stress severity.

Figures 23-26 explains the severity of normal stresses due to the unbalance force for four materials wherein the 0.1 kg of unbalanced mass added on the disk with the increasing, the frequencies from 270 to 2700 Hz with step size 100 Hz.

X-direction X-direction

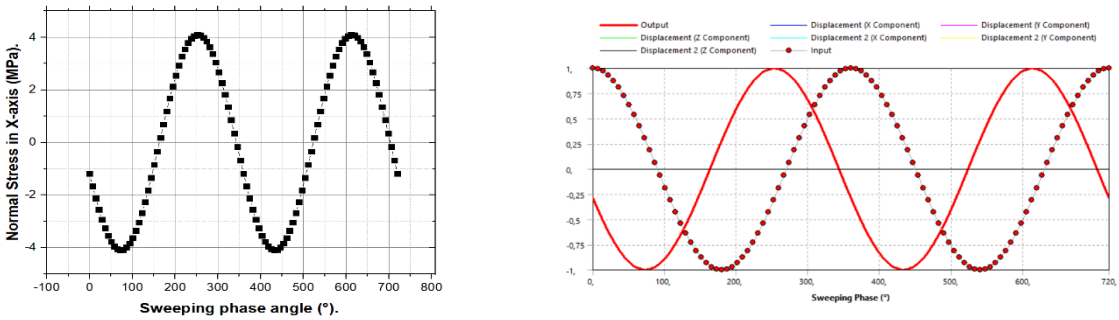

Stress severity for JIS-S45C steel in X-axis direction

Y-direction Y-direction

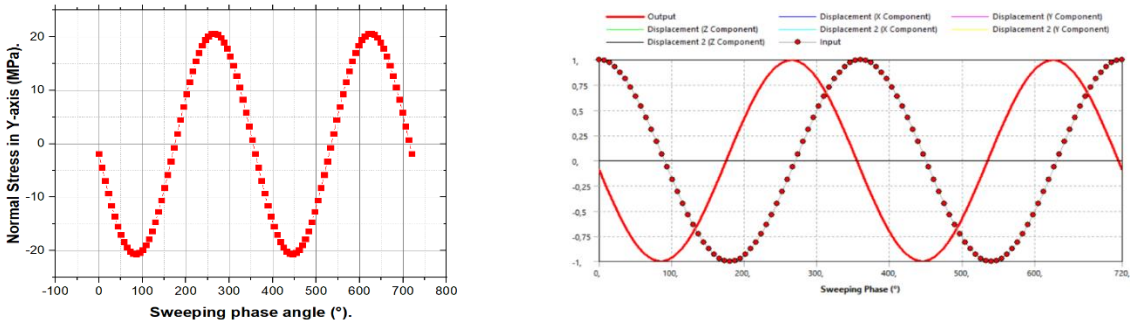

Stress severity for JIS-S45C steel in Y-axis direction

Z-direction Z-direction

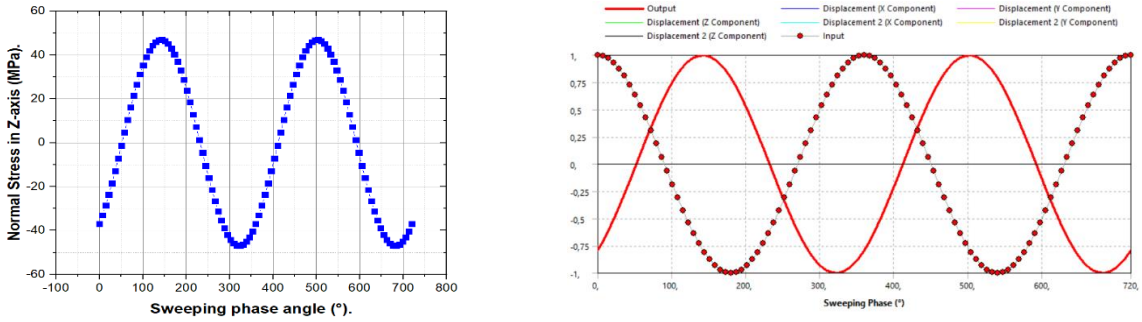

Stress severity for JIS-S45C steel in Z-axis direction

Fig. 23. Stresses severity vs phase angle for Jeffcott rotor for JIS-S45C steel material

For a steel material of JIS-S45C in X direction. The maximum normal stress is -1.186 MPa at sweep phase angle equal 0°, 4.0987 MPa at sweep phase angle equal 252°, -4.0987 MPa at sweep phase angle equals 432°, 4.0987 MPa at sweep phase angle equals 612°, -1.186 MPa at sweep phase angle equals 720° (See Fig. 23).

For a steel material of JIS-S45C in Y direction. The maximum normal stress is -1.8746 MPa at sweep phase angle equal 0°, 20.64 MPa at sweep phase angle equal 266.4°, -20.64 MPa at sweep phase angle equals 446.4°, 20.64MPa at sweep phase angle equals 626.4°, -1.8745 MPa at sweep phase angle equals 720° in Y direction (See Fig. 23).

For a steel material of JIS-S45C in Z direction. The maximum normal stress is -37.009 MPa at sweep phase angle equal 0°, 46.965 MPa at sweep phase angle equal 144°, -46.965 MPa at sweep phase angle equals 324°, 46.965 MPa at sweep phase angle equals 504°, -37.009 MPa at sweep phase angle equals 720° (see Fig. 23).

For a steel material of 38CrMoAl in X direction. The maximum normal stress is -0.97662MPa at sweep phase angle equal 0°, 2.2592MPa at sweep phase angle equal 115.2°, -2.2592MPa at sweep phase angle equals 115.2°, 2.2592MPa at sweep phase angle equals 475.2°, -0.97663MPa at sweep phase angle equals 720° (see Fig. 24).

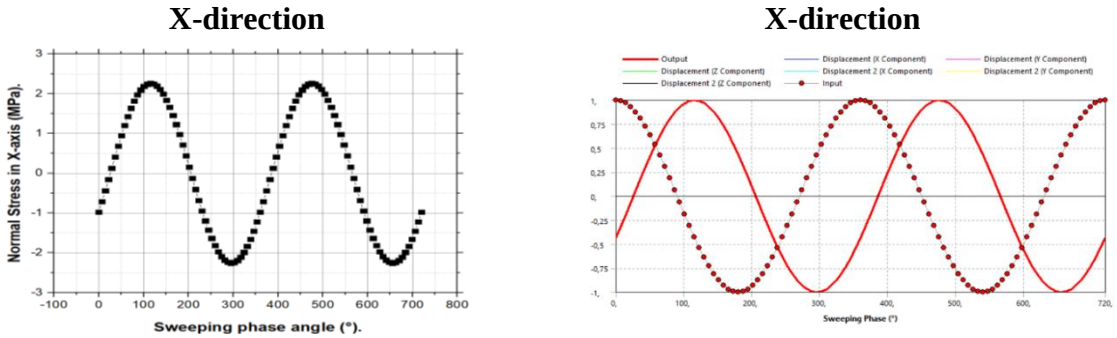

Stress severity for 38CrMoAl steel in X-axis direction

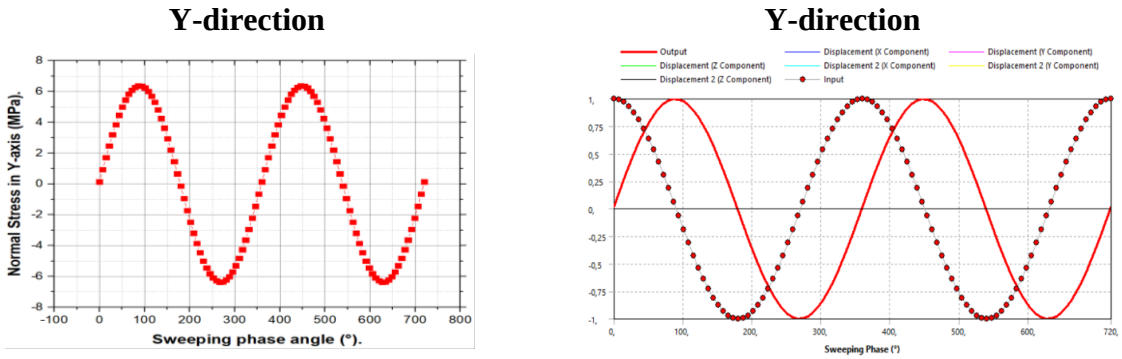

Stress severity for 38CrMoAl steel in Y-axis direction

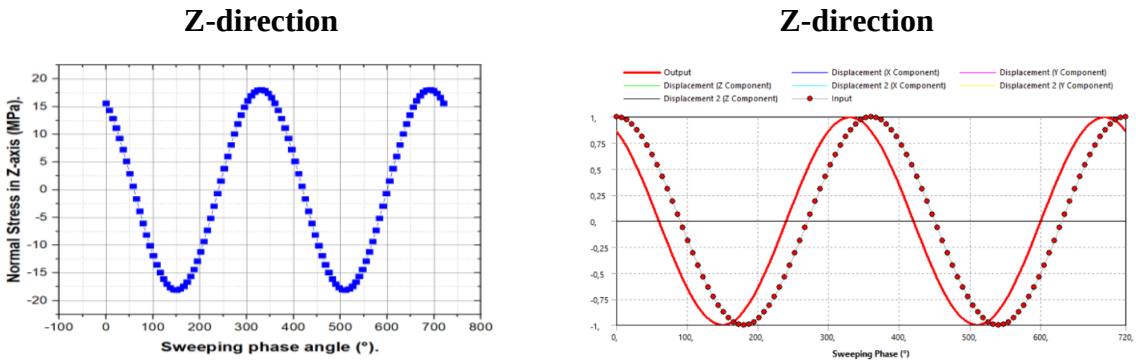

Stress severity for 38CrMoAl steel in Z-axis direction

Fig. 24. Stresses severity vs phase angle for Jeffcott rotor with 38CrMoAl steel material

For a steel material of 38CrMoAl in Y direction. The maximum normal stress is – 0.13911 MPa at sweep phase angle equal 0°, 6.3642 MPa at sweep phase angle equal 86.4°, -6.3642 MPa at sweep phase angle equals 266.4°, 6.3642 MPa at sweep phase angle equals 446.4°, -6.3642 MPa at sweep phase angle equals 626.4°, 6.3642 MPa at sweep phase angle equals 446.4°, 0,1391 MPa at sweep phase angle equals 720° in Y direction (see Fig. 24).

For a steel material of 38CrMoAl in Z direction. The maximum normal stress is 15.623 MPa at sweep phase angle equal 0°, -18.086 MPa at sweep phase angle equal 151.2°, -18,086 MPa at sweep phase angle equals 331.2°, -18.086 MPa at sweep phase angle equals 511.2°, -15.623 MPa at sweep phase angle equals 720° (See Fig. 24).

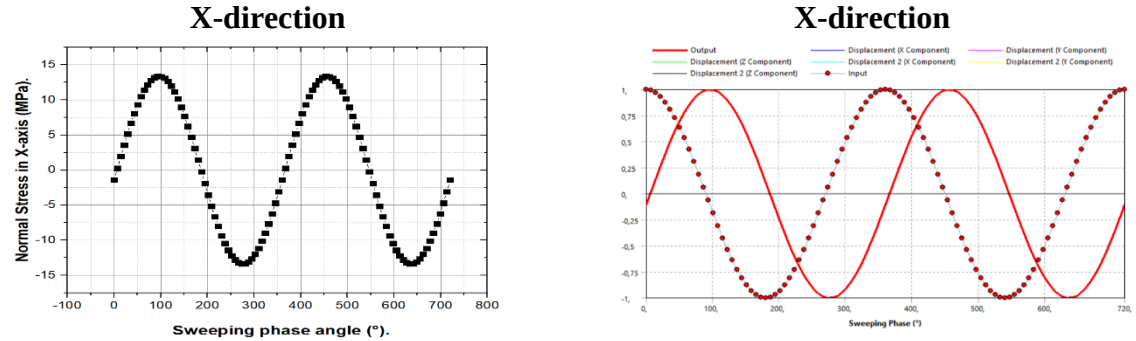

Stress severity for Structure steel in X-axis direction

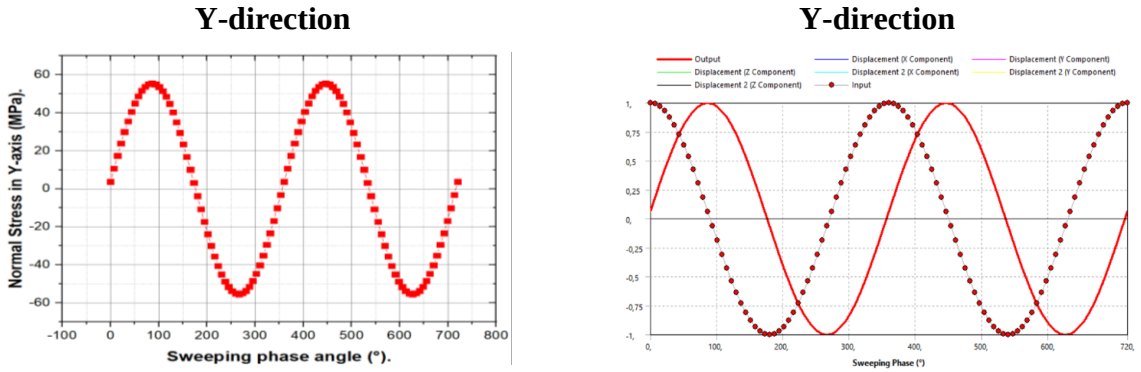

Stress severity for Structure steel in X-axis direction

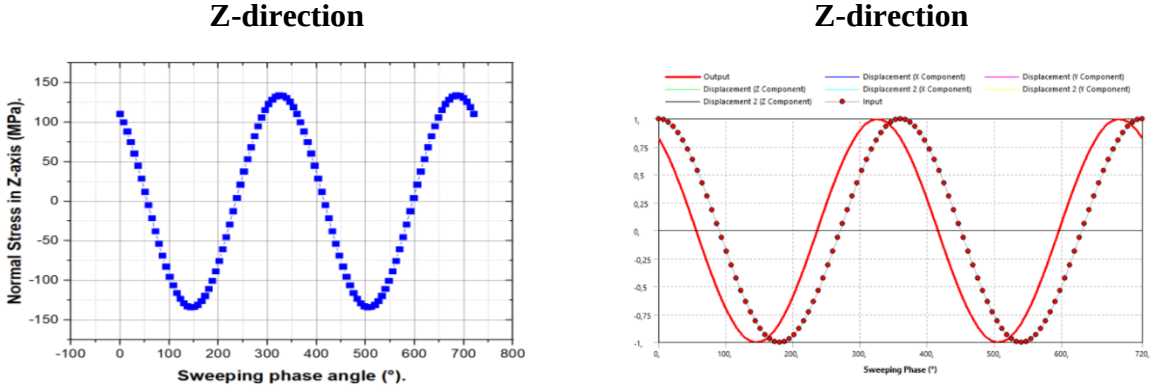

Stress severity for Structure steel in X-axis direction

Fig. 25. Stresses severity vs phase angle for Jeffcott rotor with for Structure steel material

For Structural steel material in X direction. The maximum normal stress is -1.4351 MPa at sweep phase angle equal 0°, 13.36 MPa at sweep phase angle equal 93.6°, -13.36 MPa at sweep phase angle equals 273.6°, 13.36 MPa at sweep phase angle equals 453.6°, -13.33 MPa at sweep phase angle equals 640.8°, -1.4351 MPa at sweep phase angle equals 270° (See Fig. 25).

For structural steel material in Y direction. The maximum normal stress is 3.7447 MPa at sweep phase angle equal 0°, 55.452 MPa at sweep phase angle equal 86.4°, -55.452 MPa at sweep phase angle equals 266.4°, 55,452 MPa at sweep phase angle equals

446.4°, -54.982 MPa at sweep phase angle equals 633.6°, 3.7446 MPa at sweep phase angle equals 270° (see Fig. 25).

For Structural steel material in Z direction. The maximum normal stress is 110.71 MPa at sweep phase angle equal 0°, -134.02 MPa at sweep phase angle equal 144°, 134.02 MPa at sweep phase angle equals 324°, -134.02 MPa at sweep phase angle equals 504°, 110.71MPa at sweep phase angle equals 270° (see Fig. 25).

For titanium alloy (Ti-6AL-4V) material in X direction. The maximum normal stress is -2.7244 MPa at sweep phase angle equal 0°, 7.8805 MPa at sweep phase angle equal 108°, -7.8565 MPa at sweep phase angle equals 295.2°, 7.8805 MPa at sweep phase angle equals 468°, -7.8805 MPa at sweep phase angle equals 648°, -2.7244 MPa at sweep phase angle equals 270° (see Fig. 26).

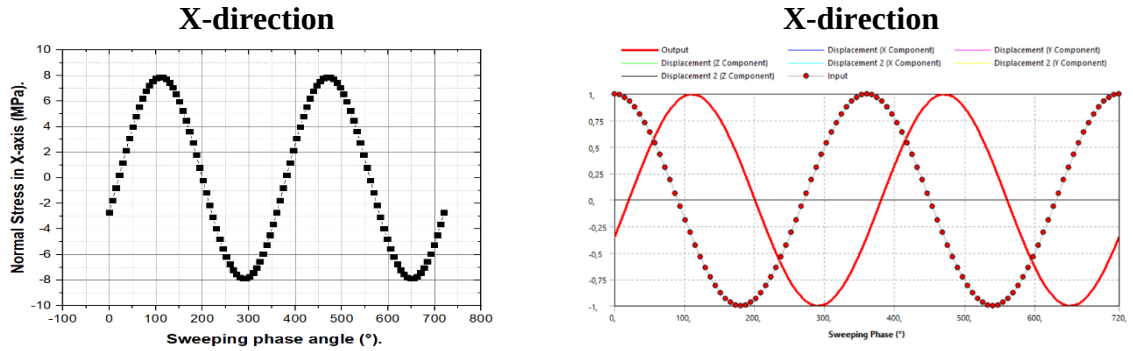

Stress severity for Titanium Alloy (Ti-6AL-4V) in X-axis direction

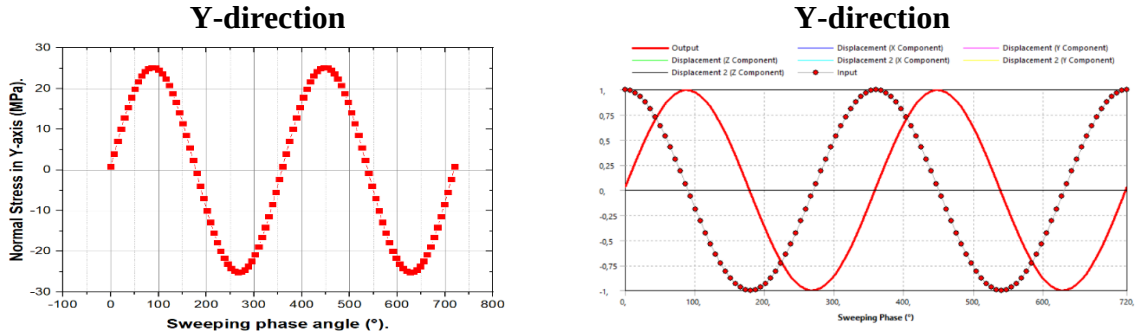

Stress severity for titanium alloy (Ti-6AL-4V) in Y-axis direction

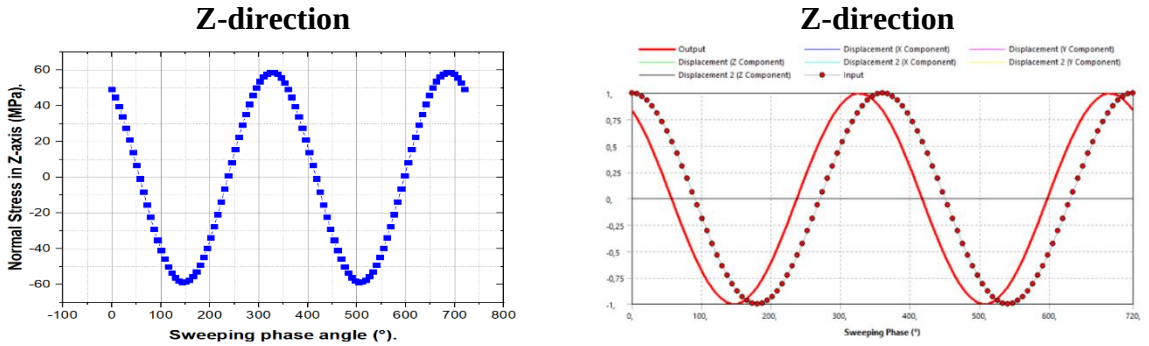

Stress severity for titanium alloy (Ti-6AL-4V) in Z-axis direction

Fig. 26. Stresses severity vs phase angle for Jeffcott rotor for Titanium Alloy (Ti-6AL-4V) material

For Titanium Alloy (Ti-6AL-4V) material in Y direction. The maximum normal stress is 0.81197MPa at sweep phase angle equal 0°, 25.16 MPa at sweep phase angle equal 86.4°, -25.16MPa at

sweep phase angle equals 266.4°, 25.16 MPa at sweep phase angle equals 446.4°, -25.16MPa at sweep phase angle equals 626.4°, 0.8119 MPa at sweep phase angle equals 270° (see Fig. 26).

For Titanium Alloy (Ti-6AL-4V) material in Z direction. The maximum normal stress is 49.207 MPa at sweep phase angle equal 0°, -58.755 MPa at sweep phase angle equal 144°, 58.755 MPa at sweep phase angle equals 324°, -58.755 MPa at sweep phase angle equals 504°, 49.207 MPa at sweep phase angle equals 270° (see Fig. 26).

Force reaction effect on Jeffcott rotor. Figure 27 explains the force reaction in the two bearings due to the unbalance force for four materials. When the 0.1 kg of unbalanced mass added on the disk with the increasing, the frequencies from 270 to 2700 Hz with step size 100 Hz.

For a material of JIS-S45C steel. When 0.1 kg of unbalance is added to the disk with the increase in frequencies from 270 to 2700 Hz with a step of 100 Hz, the maximum amplitude of reaction force along X varies from 2228.3 N at 270 Hz, 2.124E+5 N at 1350 Hz and 9.7022E5 N at 2700 Hz a shown in Fig. 27**.**

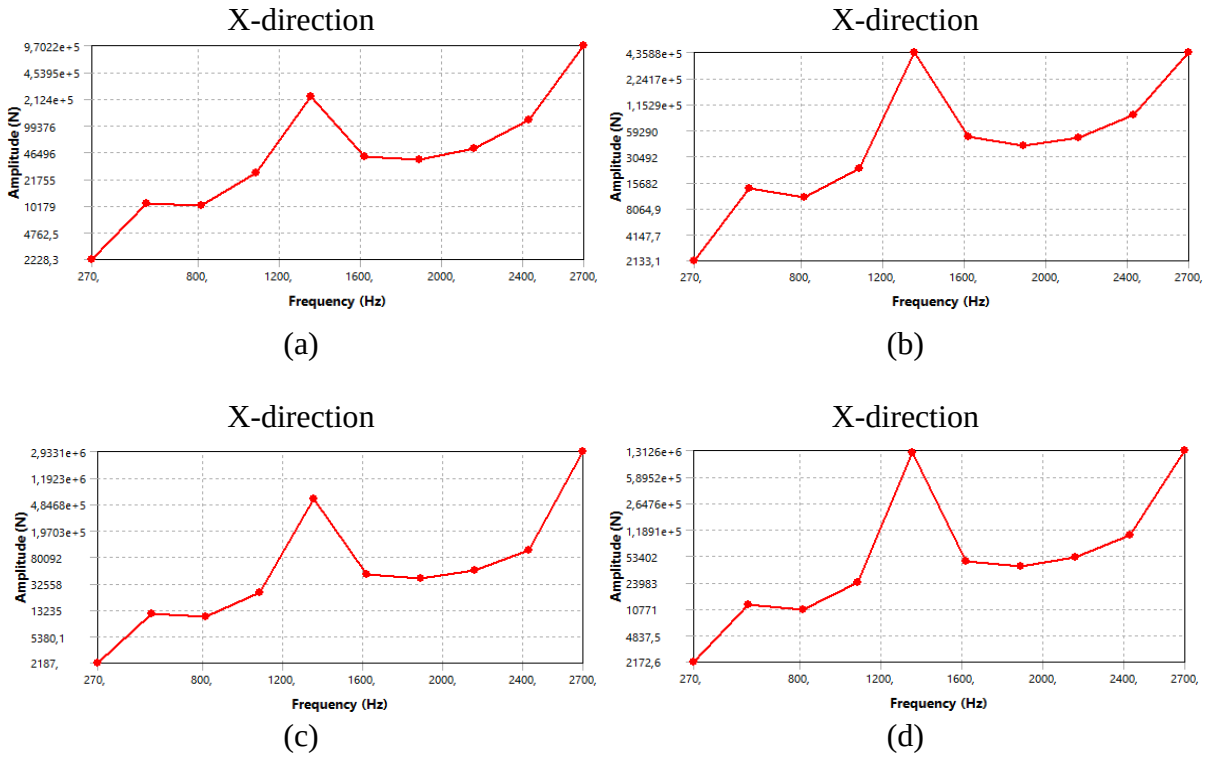

Fig. 27. Shows the Force Reaction vs phase angle for a Jeffcott rotor with 4 varieties of materials. (a) JIS-S45C; (b) 38CrMoAl; (c) structural steel; (d) Ti-6AL-4V

For a material of 38CrMoAl steel. When 0.1 kg of unbalance is added to the disk with the increase in frequencies from 270 to 2700 Hz with a step of 100 Hz, the maximum amplitude of reaction force along X varies from 2133.1 N at 270 Hz, 4.3588E+5 N at 1350 Hz and 4.3588E+5 N at 2700 Hz a shown in Fig. 27.

For a material of structural steel. When 0.1 kg of unbalance is added to the disk with the increase in frequencies from 270 to 2700 Hz with a step of 100 Hz, the maximum amplitude of reaction force along X varies from 2187 N at 270 Hz, 4.8468E+5 N at 1350 Hz and 2.9331E6 N at 2700 Hz a shown in Fig. 27.

For material of titanium alloy (Ti-6AL-4V). When 0.1 kg of unbalance is added to the disk with the increase in frequencies from 270 to 2700 Hz with a step of 100 Hz, the maximum amplitude of reaction force along X varies from 2172.6 N at 270 Hz, 1.3126E+6 N at 1350 Hz and 1.3126E+6 N at 2700 Hz a shown in Fig. 27.

For a material of JIS-S45C steel. When 0.1 kg of unbalance is added to the disk with the increase in frequencies from 270 to 2700 Hz with a step of 100 Hz, the maximum amplitude of reaction force along Y varies from 2225.1 N at 270 Hz, 2.1749E+5 N at 1350 Hz and 1.0018E+6 N at 2700 Hz a shown in Fig. 28**.**

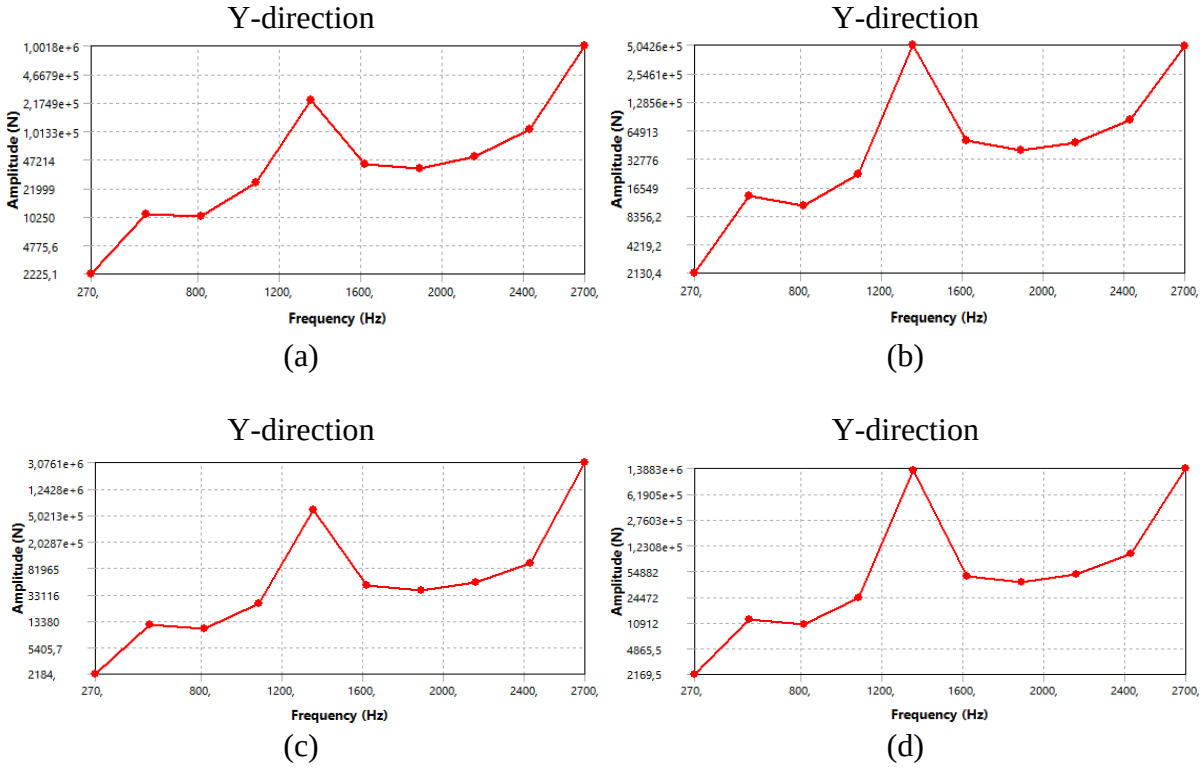

Fig. 28. Shows the deformation vs phase angle for a Jeffcott rotor with 4 varieties of materials. (a) JIS-S45C; (b) 38CrMoAl; (c) structural steel; (d) Ti-6AL-4V

For a material of 38CrMoAl steel. When 0.1 kg of unbalance is added to the disk with the increase in frequencies from 270 to 2700 Hz with a step of 100 Hz, the maximum amplitude of reaction force along Y varies from 2130.4 N at 270 Hz, 5.0426E+5 N at 1350 Hz and 5.0426 N at 2700 Hz a shown in Fig. 28.

For a material of Structural steel. When 0.1 kg of unbalance is added to the disk with the increase in frequencies from 270 to 2700 Hz with a step of 100 Hz, the maximum amplitude of reaction force along Y varies from 2184 N at 270 Hz, 5.0213E+5 N at 1350 Hz and 3.0761E+6 N at 2700 Hz a shown in Fig. 28.

For material of Titanium Alloy (Ti-6AL-4V). When 0.1 kg of unbalance is added to the disk with the increase in frequencies from 270 to 2700 Hz with a step of 100 Hz, the maximum amplitude of reaction force along Y varies from 2169.5N at 270 Hz, 1.3883E+6 N at 1350 Hz and 1.3883E+6N at 2700 Hz a shown in Fig. 28.

For a material of JIS-S45C steel. When 0.1 kg of unbalance is added to the disk with the increase in frequencies from 270 to 2700 Hz with a step of 100 Hz, the maximum amplitude of reaction force along Z varies from 3.212N at 270 Hz, 2278.7N at 1350 Hz and 2278.7E+6 at 2700 Hz a shown in Fig. 29.

For a material of 38CrMoAl steel. When 0.1 kg of unbalance is added to the disk with the increase in frequencies from 270 to 2700 Hz with a step of 100 Hz, the maximum amplitude of reaction force along Z varies from 2.7424 N at 270 Hz, 3787.3 N at 1350 Hz and 1533.9 N at 2700 Hz a shown in Fig. 29.

For a material of structural steel. When 0.1 kg of unbalance is added to the disk with the increase in frequencies from 270 to 2700 Hz with a step of 100 Hz, the maximum amplitude of reaction force along Z varies from 2.9805N at 270 Hz, 4425.6N at 1350 Hz and 1776.3N at 2700 Hz a shown in Fig. 29.

For material of titanium alloy (Ti-6AL-4V). When 0.1 kg of unbalance is added to the disk with the increase in frequencies from 270 to 2700 Hz with a step of 100 Hz, the maximum amplitude of reaction force along Z varies from 2.8215 N at 270 Hz, 9544.7 N at 1350 Hz and 1251.5 N at 2700 Hz a shown in Fig. 29.

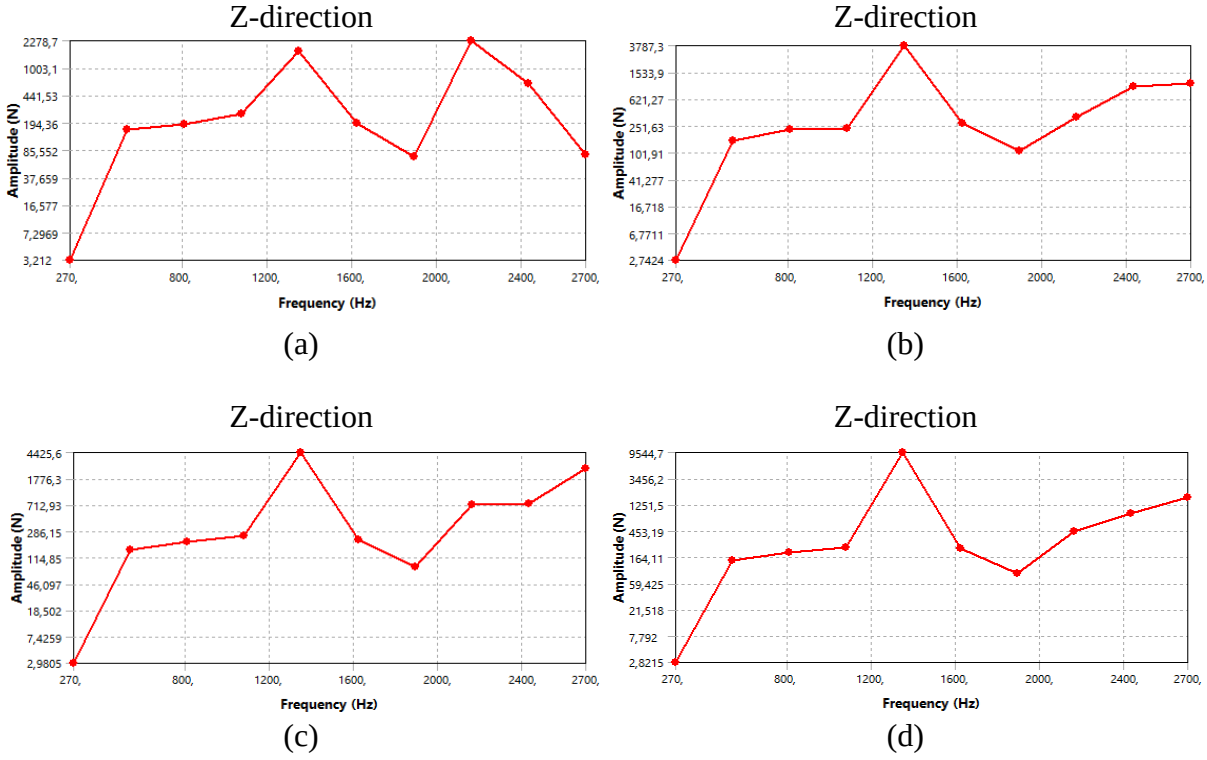

Fig. 29. Shows the force reaction for a Jeffcott rotor with 4 varieties of materials: (a) JIS-S45C; (b) 38CrMoAl; (c) structural steel; (d) Ti-6AL-4V

Distribution of equivalent stress and total displacement in rotordynamic system. Figure 30 shows the equivalent stress distribution in Jeffcott's rotor-dynamic system (JIS S45C, 38CrMoAl, structural steel, titanium alloy) for four different materials. When 0.1 kg of unbalance is added to the disc with the increase in frequencies from 270 to 2700 Hz with a step of 100 Hz, the amplitude of maximum equivalent stresses for 4 materials are equal to (18625, 9435.2, 55134, 23624 MPa) (red outline at bearing level).

On the other hand, when 0.1 kg of unbalance is added to the disk with the increase of frequencies from 270 to 2700 Hz with a step of 100 Hz, the normal plastic deformation amplitude for 4 materials (JIS S45C, 38CrMoAl, structural steel, titanium alloy) are equal to (0.1026, 0.0506, 0.2894, 0.2187 mm/mm).

We note in Fig. 30, the single-disc root-dynamic system manufactured by the two materials (JIS S45C, 38CrMoAl) show a minimum total displacement which are equal to (11.984, 5.213 mm) by contribution of the two steels (structural steel, titanium alloy).

Figure 30 shows the maximum shear stress distribution in Jeffcott's rotor-dynamic system made by four different materials (JIS S45C, 38CrMoAl, structural steel, titanium alloy). When 0.1 kg of unbalance is added to the disc with increasing frequencies from 270 to 2700 Hz with a step of 100 Hz, the maximum shear stress amplitude for 4 materials are equal to (10036, 5288, 29634, 12649 MPa) (outline in red at the bearings).

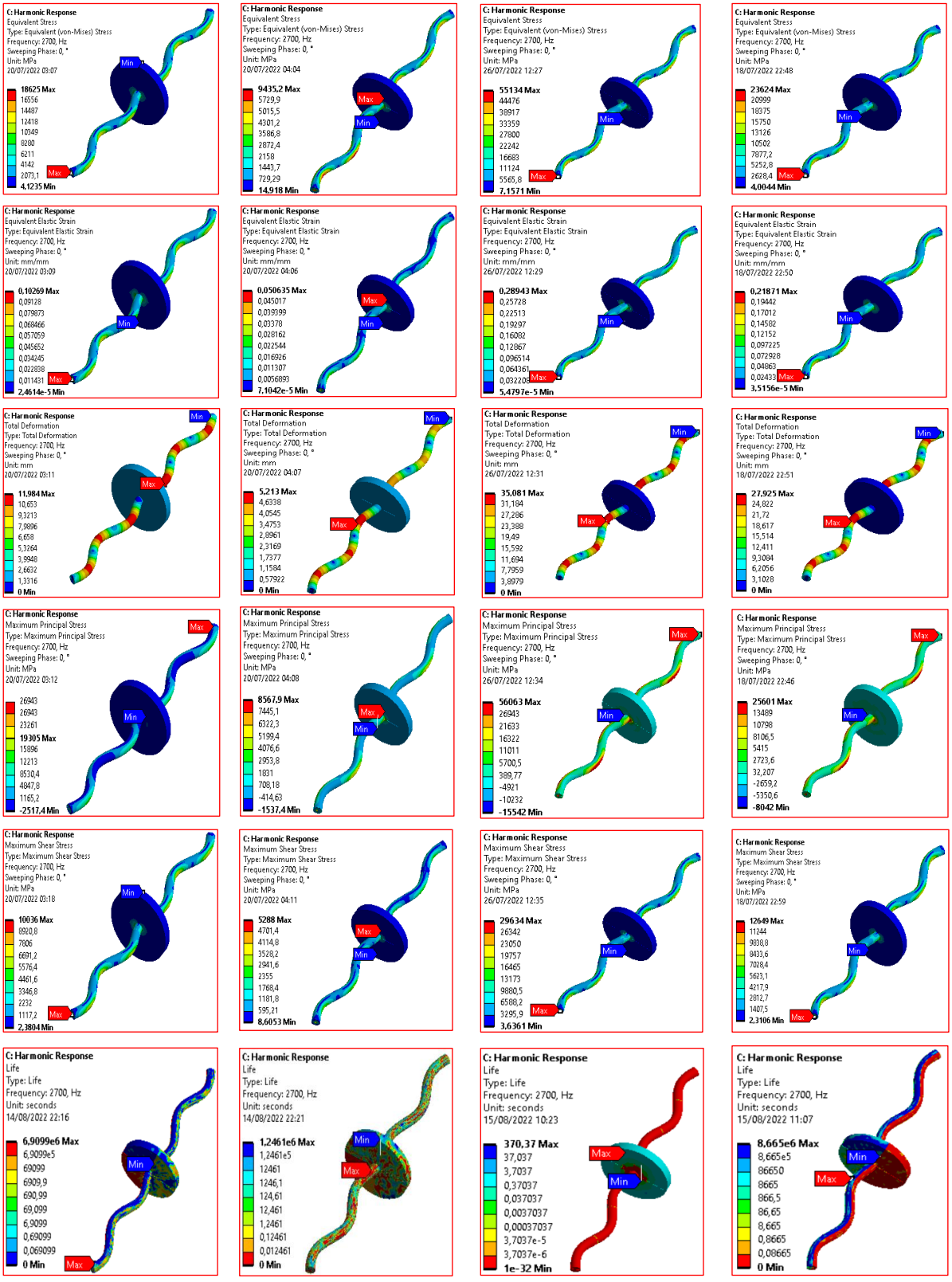

JIS-S45C steel **38CrMoAl** **Structural steel** **Titanium**

Fig. 30. Shows the von Mises stress, normal elastic strain, total displacement, maximum shear stress and life cycle number for a Jeffcott rotor with 4 varieties of materials.

On the other hand, when 0.1 kg of unbalance is added to the disc with the increase in frequencies from 270 Hz to 2700 Hz with a step of 100 Hz, the number of life cycles for the 4 materials (JIS S45C, 38CrMoAl, Structural Steel, Titanium Alloy) are equal to (6.9099e6, 1.2461e6, 370.37, 8.665e6).

Conclusions

The academic finite element method is a good tool to understand the dynamics of rotor system. It is observed that all the verification of analysis, that of numerical results for a single rotor system is very good agreement with ANSYS results. The Jeffcott rotor performed using the commercially available ANSYS Workbench software indicated that the critical velocities for four materials are 1784.2, 1784.9, 8147.7RPMs for JIS S45C steel material, 1858.7, 1859.4, 8468.1 RPMs for 38CrMoAl steel material, 1813.9, 1814.6, 8275,9 RPMs for structural steel material and 1824.8, 1825.5, 8323.9 for titanium Alloy (Ti-6AL-4V) material. The natural frequencies of the Jeffcott rotor are also higher for 38CrMoAl steels and are equal for the two materials (titanium alloy (Ti-6Aal-4V) and JIS S45C) and minimum for steel structure steels.

For JIS-S45C steel a stability of the Jeffcott rotor system found in the Campbell diagram between the two critical speeds (1784.2 rpm, 8147.7 RPM), that is to say the rotor system is turned well with a speed rotation superior to 1784.2 rpm and lower of 8147.7 rpm. On the other hand, if the rotation speed of the dynamic rotor superior the critical speed 8147.7 RPM, the rotor system is turned well (see Fig. 12).

For 38CrMoAl steel a stability of the Jeffcott rotor system found in the Campbell diagram between the two critical speeds (1858.7 rpm, 8468.1 rpm), that is to say the rotor system is turned well with a speed rotation superior of 1858.7 rpm and lower of 8468.1 rpm. On the other hand, if the rotation speed of the dynamic rotor superior the critical speed 8468.1 rpm, the rotor system is turned well (see Fig. 12).

For structural steel a stability of the Jeffcott rotor system found in the Campbell diagram between the two critical speeds (1813.9, 8275.9 rpm), that is to say the rotor system is turned well with a speed rotation superior of 1813,9rpm and lower of 8275.9 rpm. On the other hand, if the rotation speed of the dynamic rotor superior the critical speed 8275.9 rpm, the rotor system is turned well (see Fig. 12).

For titanium alloy (Ti-6AL-4V) material a stability of the Jeffcott rotor system found in the Campbell diagram between the two critical speeds (1824.8, 8323.9 rpm), that is to say the rotor system is turned well with a speed rotation superior of 1824.8rpm and lower of 8323.9 rpm. On the other hand, if the rotation speed of the dynamic rotor superior the critical speed 8323.9 rpm, the rotor system is turned well (see Fig. 12). The rotary machines undergoing higher operating speeds like propeller shafts, turbine and compressor are recommended to use JIS S45C and Ti-6AL-4V.

In the harmonic analysis, due to the unbalance force of 0.1 kg acting on the disc, the vibration severity is very high for the steel materials, and Equivalent stress is 18625 MPa for JIS S45C steel material, 9435.2 MPa for 38CrMoAl steels material, and 55134 MPa for Structural steels material, and 23624 MPa for titanium alloy (Ti-6AL-4V) material.

Not only equivalent alternating stresses but also the other stresses in the X-axis, Y-axis, and Z-axis directions are less severity for 38CrMoAl steels materials compared to the JIS S45C steels, 38CrMoAl steels and titanium alloy (Ti-6AL-4V) materials (refer Figs. 10–12). The rotary machines undergoing high stress severity and deformation severity are recommended to use 38CrMoAl steels.

Rotor dynamic analysis of Jeffcott rotor with four materials, JIS S45C, 38CrMoAl, structural steel, titanium alloy materials are highly recommended with the less severity of vibration. Choose JIS S45C and Ti-6AL-4V materials for higher whirling speeds compared to structural steel, titanium alloy materials.

The sweeping phase angle severity is found maximum on the Z-direction for all materials. Compared to the two steels (structural steels, titanium alloy), parameters such as natural

frequency, the harmonic response is far better for (JIS S45C, 38CrMoAl) and are recommended. A tabular representation is listed in Table 2 and 3.

Authors thus presented a comparative picture about dynamic analysis of Jeffcott rotor with 0.1 kg of unbalance mass is added to the disc, as a case sample application. It is expected that a study capturing the comparative status of different engineering materials along with different analyses will be useful for both researchers and practitioners. Both communities will be motivated to explore and compare different materials for diverse and better applications.

References

1. Malgol A, Potdar Y. Modelling and simulation of single rotor system. *Int J Latest Technol Eng Manage Appl Sci*. 2017;6(4): 163–169.
2. Tai X, Ma H, Liu F, Liu Y, Wen B. Stability and steady-state response analysis of a single rub-impact rotor system. *Archive of Applied Mechanics*. 2015;85(1): 133–148.
3. Wang N, Jiang D. Vibration response characteristics of a dual-rotor with unbalance-misalignment coupling faults: Theoretical analysis and experimental study. *Mechanism and Machine Theory*. 2018;125: 207–219.
4. Xul J, Zheng X, Zhang J, Liu, X. Vibration characteristics of unbalance response for motorized spindle system. *Procedia Engineering*. 2017;174: 331–340.
5. Ghoneam SM, Asy MA, Embaby AG, Elhadhody EA. Dynamic analysis of rotor system with active magnetic bearings using finite element method. *International Journal of Engineering Applied Sciences and Technology*. 2022;7(1): 2455–2143.
6. Sghaier E, Bourdon A, Remond, Dion JL, Peyret N. Dynamic behavior of very-high speed rotors at non-stationary conditions. *Proceedings of The 10th International Conference On Rotor Dynamics – Iftomm*. 2019;4(63): 79–90.
7. Chen Y, Mendoza A.S.E, & Griffith D.T. Experimental and numerical study of high-order complex curvature mode shape and mode coupling on a three-bladed wind turbine assembly. *Mechanical Systems and Signal Processing*. 2021;160: 107873.
8. Dabachi MA, Rouway M, Rahmouni A, Bouksour O, Sbai SJ, Laaouidi H, Lagdani O. Numerical investigation of the structural behavior of an innovative offshore floating darrieus-type wind turbines with three-stage rotors. *Journal of Composites Science*. 2022;6(6): 167.
9. Bose A, Sathujoda P, Canale G. Natural frequency analysis of a functionally graded rotor-bearing system with a slant crack subjected to thermal gradients. *International Journal of Turbo & Jet-Engines.* 2021. Available from: https://doi.org/10.1515/tjeng-2021-0002
10. Sudhakar GNDS, Sekhar AS. Identification of unbalance in a rotor bearing system. *Journal of Sound and Vibration*. 2011;330(10): 2299–2313.
11. Shrivastava A, Mohanty AR. Identification of unbalance in a rotor system using a joint input-state estimation technique. *Journal of Sound and Vibration*. 2019;442: 414–427.
12. Pavlenko IV, Simonovskiy VI, Demianenko MM. Dynamic analysis of centrifugal machines rotors supported on ball bearings by combined application of 3D and beam finite element models. *IOP Conference Series: Materials Science and Engineering*. 2017;233(1): 012053.
13. Fernandes R, El-Borgi S, Ahmed K, Friswell MI, Jamia N. Static fracture and modal analysis simulation of a gas turbine compressor blade and bladed disk system. *Advanced Modeling and Simulation in Engineering Sciences*. 2016;3: 1–23.
14. Jung HC, Krumdieck S. Rotordynamic modelling and analysis of a radial inflow turbine rotor-bearing system. *International Journal of Precision Engineering and Manufacturing*. 2014;15: 2285–2290.
15. Sghaier E, Bourdon A, Remond D, Dion JL, Peyret N. Dynamic behavior of very-high speed rotors at non-stationary conditions. In: *International Conference on Rotor Dynamics*. 2018. p.79–90.
16. Yang XU, Lei Z, Suyuan YU. *Dynamics Analysis of very flexible Rotor. Technical Paper*. Beijing: Institute of Nuclear Energy Technology, Tsinghua University; 2004.

17. Egusquiza E, Valero C, Presas A, Huang X, Guardo A, Seidel U. Analysis of the dynamic response of pump-turbine impellers. Influence of the rotor. *Mechanical Systems and Signal Processing*. 2016;68: 330–341.
18. Garcia M, Laín S, Orrego S, Barbosa J, Quintero B. Hydraulic and rotor-dynamic interaction for performance evaluation on a Francis turbine. *International Journal on Interactive Design and Manufacturing (IJIDeM)*. 2017 ;11(3): 623–632.
19. Vasquez RE. On the use of structural dynamics in virtual manufacturing. *International Journal on Interactive Design and Manufacturing (IJIDeM)*. 2017;11(1): 103–114.
20. Newland DE, Ungar EE. *Mechanical vibration analysis and computation*. 1990.
21. Rao S.S. *Vibration of continuous systems*. John Wiley & Sons; 2019.
22. Kushwaha N, Patel V.N. Modelling and analysis of a cracked rotor: a review of the literature and its implications. *Archive of Applied Mechanics*. 2020;90(6): 1215–1245.
23. Sarmah N, Tiwari R. Dynamic analysis and identification of multiple fault parameters in a cracked rotor system equipped with active magnetic bearings: a physical model based approach. *Inverse Problems in Science and Engineering*. 2020;28(8): 1103–1134.
24. Jung H.C, Krumdieck S. Rotordynamic modelling and analysis of a radial inflow turbine rotor-bearing system. *International Journal of Precision Engineering and Manufacturing*. 2014;15(11): 2285–2290.
25. Lalanne M, Ferraris G. *Rotordynamics prediction in engineering*. Wiley; 1990.
26. Rao JS. *History of rotating machinery dynamics*. Springer; 2011.
27. Alam HS, Irasari P. Rotor-dynamic characteristic evaluation of interior permanent magnet motor using finite element method. *Journal of Mechatronics, Electrical Power, and Vehicular Technology*. 2014;5(1): 1–8.
28. Santiago DFA. *Diagnostic of faults of rotating machinery using wavelet transform and artificial neural networks (Doctoral dissertation, Phd Thesis, am inas acu ldade de ngen aria ec nica)*. Universidade Estadual de Campinas; 2003.
29. Lalanne M, Ferraris G. *Rotordynamics prediction in engineering*. John Wiley & Sons; 1998.
30. Senko R, Silva AA, Borges JM. Dynamic and control of a rotor system based on passage through critical speeds with incorporation of smart actuators in flexible bearing device. In*: Proceedings of Congresso Brasileiro de Engenharia Mecânica-COBEM*. Ribeirão Preto; 2013.

THE AUTHORS

Nasreddine El bachir Afane
e-mail: afanenasreddine@gmail.com

Samir Zahaf
e-mail : samir.zahaf@univ-dbkm.dz

Mouloud Dahmane
e-mail: m.dahmane@ensh.dz

Azzeddine Belaziz
e-mail: belaziz2013@gmail.com

Rachid Noureddine
e-mail : noureddine.rachid@univ-oran2.dz